Max-Planck-Institut für Meteorologie
Max Planck Institute for Meteorology

MAX-PLANCK-GESELLSCHAFT

Held-Suarez Test with ECHAM5

Hui Wan, Marco A. Giorgetta, Luca Bonaventura

Reports on Earth System Science

Held-Suarez Test with ECHAM5

Hui Wan, Marco A. Giorgetta, Luca Bonaventura

Hamburg 2006

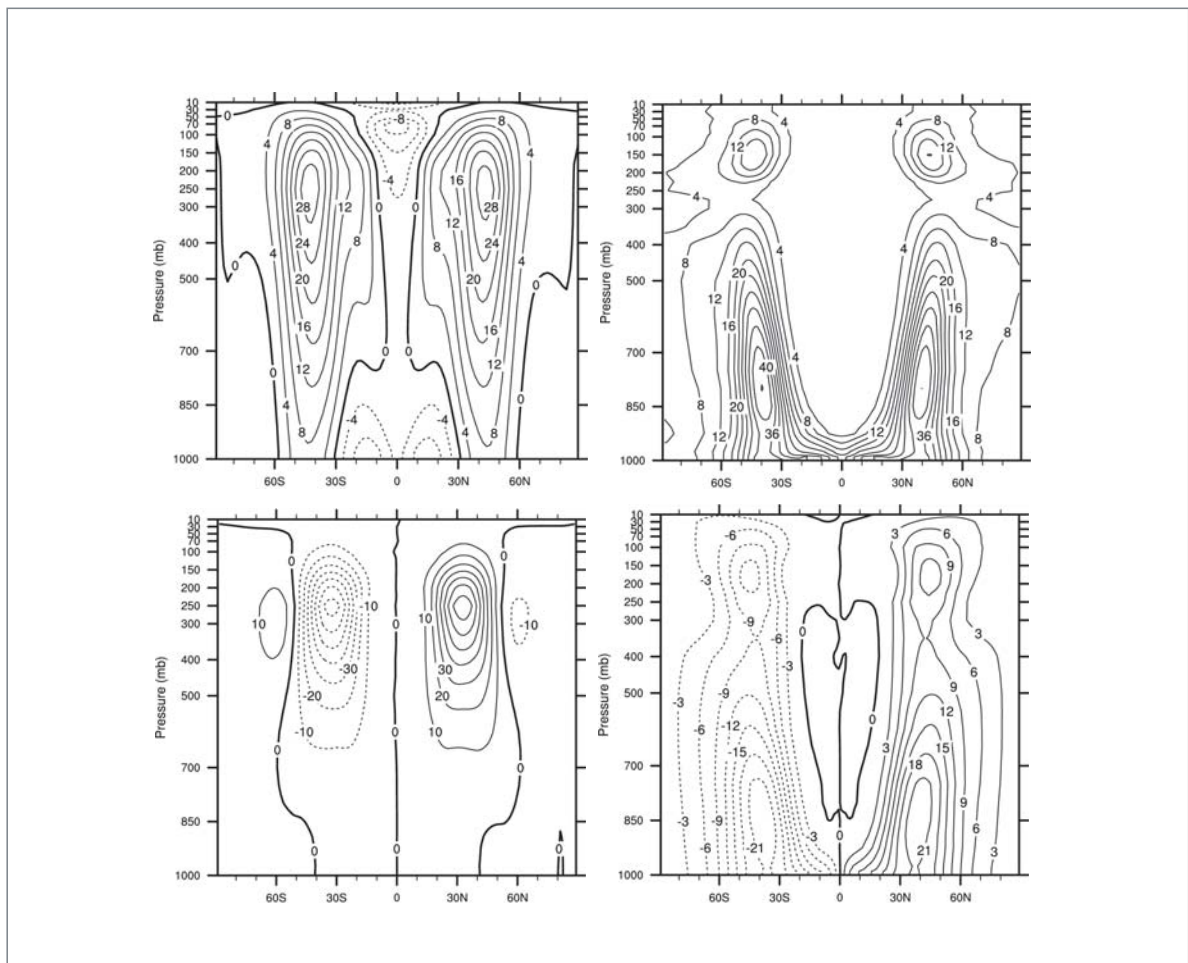Hui Wan[1] ∎ Marco A. Giorgetta[1] ∎ Luca Bonaventura[2]

1

Max-Planck-Institut für Meteorologie
Bundesstrasse 53
20146 Hamburg
Germany

2

MOX-Dipartimento di Matematica
Politecnico di Milano
Milano, Italy

Held-Suarez Test with ECHAM5

Hui Wan, Marco A. Giorgetta, Luca Bonaventura

Hamburg 2006

Held-Suarez Test with ECHAM5

Hui Wan[1], Marco A. Giorgetta[1], Luca Bonaventura[2]

[1] Max Planck Institute for Meteorology, Hamburg, Germany
[2] MOX-Dipartimento di Matematica, Politecnico di Milano, Milano, Italy

Abstract

The idealized test case proposed by Held and Suarez (1994) is carried out with the ECHAM5 model. A long-term integration at a medium resolution (T42L19) is performed first to investigate the internal variability of the test case and the memory of the simulated climate state. Based on the results, ensemble experiments are conducted at various spatial and temporal resolutions, aiming at evaluating the sensitivity of the dynamical core of ECHAM5 and numerical convergence of the solutions. It is found that increase of horizontal resolution leads to slight weakening and poleward shift of the westerly jets as well as warming in the high latitudes. Baroclinic wave activities steadily intensify with increased horizontal resolution, as indicated by significant enhancement of the transient eddy temperature variance and eddy kinetic energy. Increase of vertical resolution from L19 to L31 leads to even stronger eddy variances as well as equatorward shift of the westerly jets. There is considerable cooling near the tropical tropopause and warming in the polar upper troposphere and lower stratosphere. Further refinement of the spatial grid does not lead to differences that are judged to be significant by the statistical test, indicating the convergence of solutions at T85L31 resolution. Time step does not have much influence on the simulated climate state within the selected range in this idealized case. Differences between integrations with various time steps are just within the noise level induced by the inherent variability. Single-realization experiments proceeding 1200 days are also performed, in which the main features of the simulated 1000-day climate are found in good agreement with many other models, although some differences are also detectable.

1 Introduction

In the area of climate modelling, sensitivity of simulated climate to increased spatial resolution is a topic of both scientific interest and practical value. There have been a number of studies on this issue using various models. Examples are experiments performed by Boyle (1993) and Phillips et al. (1995) with the operational forecast model of the European Centre for Medium-range Weather Forecasts (ECMWF), Williamson et al. (1995) with the climate model of the National Centre for Atmospheric Research (NCAR) of the United States, Stratton (1999), Pope et al. (2001) and Pope and Stratton (2002) with the climate model of the Hadley Centre. Roeckner et al. (2006) performed a series of AMIP-style (Atmospheric Model Intercomparison Project, Gates et al., 1999) experiments using the most recent version of the Max Planck Institute for Meteorology

atmospheric general circulation model, ECHAM5, with resolutions ranging from T21L19 to T159L31. Among many others, these studies use full atmospheric models with various physics parameterizations included. Mixed results are obtained and some aspects of the convergence properties were found to be model dependent. Complex interactions between the dynamical part and physics parameterizations of the models make it difficult to untangle the intertwined effects. To reduce the complexity, it may be helpful to concentrate on the dynamical parts first. In this study, we investigate this specific issue with the ECHAM5 model: given a "perfect" parameterization, how do the solutions of the dynamical core behave at different resolutions?

The problem for testing the dynamical core results from the fact that there are no exact solutions of the primitive equations with realistic forcing. Without the aid of analytic solutions, identifying and quantifying errors in the three-dimensional numerical models is difficult. In recent years, a test case proposed by Held and Suarez (1994) has met considerable acceptance. In this test case, physics parameterization schemes of the full climate models are replaced by prescribed forcing and dissipation. The test case is simple by design, but forces the models to produce circulations that are reasonably realistic in many aspects. Many modeling groups have been using this test case as the first step of validation and intercomparison of the dynamical cores of global atmospheric models. Previous studies have used this test case to investigate the convergence of dynamical cores with increased horizontal resolution (e.g. Boer and Denis 1997), to explain differences between Eulerian and semi-Lagrangian dynamics (Chen et al 1997) and to investigate the sensitivity to vertical resolution (Williamson et al. 1998). Jablonowski (1998) and Ringler et al. (2000) reported in detail the responses of new geodesic dynamical cores at different horizontal resolutions. Pope and Stratton (2002) used this idealized test to help to determine the processes governing horizontal resolution sensitivities in the HadAM3 model. In these studies, the Held-Suarez test case has been implemented in different ways for different purposes. In most cases, the proposal by Held and Suarez (1994), namely obtaining the model climate from the last 1000 days of a 1200-day integration, is adopted, while shorter integrations are used in some other studies (e.g. Ringler et al., 2000). Boer and Denis (1997) and Jablonowski (1998) subdivided a 1200-day integration to shorter periods to get independent realizations for their analysis. So far, there has been no specific discussion on the implementation strategy which is based on the inherent properties of the atmospheric motions in this test case.

In the present study, the Held-Suarez idealized forcing is implemented in the ECHAM5 model. A long-term integration (about 60 years) at a medium resolution (T42L19) is carried out first to investigate the internal variability of this test case and the memory of the simulated climate state. Based on these analyses, ensemble simulations are carried out at various spatial and temporal resolutions, aiming at evaluating the sensitivity of the dynamical core and numerical convergence of the solutions. Single-realization experiments are also performed in the traditional way to provide results that can be directly compared with other models.

The report is organized as follows. Section 2 and 3 are brief introductions to the Held-Suarez test case and the dynamical core of ECHAM5, respectively. Section 4 is the analysis on the internal variability of the Held-Suarez test case. Section 5 describes in detail the experiments and methodologies used for evaluating the convergence of the solutions. The results are discussed in section 6. Section 7 compares the simulations of ECHAM5 with some other models. Section 8 gives the conclusions.

2 The Held-Suarez test case

In the Held-Suarez test case, a simple Newtonian relaxation of the temperature field to a zonally symmetric state is used as the diabatic forcing term for the thermodynamic equation. Rayleigh damping of low-level winds representing boundary-layer friction is imposed as forcing and dissipation term in the momentum equation. The detailed specifications are as follows (Held and Suarez 1994):

$$\frac{\partial \vec{V}}{\partial t} = \ldots - k_v(\sigma)\vec{V}$$

$$\frac{\partial T}{\partial t} = \ldots - k_T(\phi,\sigma)\left[T - T_{eq}(\phi,p)\right]$$

$$T_{eq} = \max\left\{200K, \left[315 - (\Delta T)_y \sin^2\phi - (\Delta\theta)_z \log\left(\frac{p}{p_0}\right)\cos^2\phi\right]\left(\frac{p}{p_0}\right)^\kappa\right\}$$

$$k_T = k_a + (k_s - k_a)\max\left(0, \frac{\sigma - \sigma_b}{1 - \sigma_b}\right)\cos^4\phi$$

$$k_v = k_f \max\left(0, \frac{\sigma - \sigma_b}{1 - \sigma_b}\right)$$

$$k_f = 1 \ day^{-1} \qquad\qquad \sigma_b = 0.7$$

$$k_a = 1/40 \ day^{-1} \qquad\qquad (\Delta T)_y = 60K$$

$$k_s = 1/4 \ day^{-1} \qquad\qquad (\Delta\theta)_z = 10K$$

$$\kappa = \frac{R}{C_p} = \frac{2}{7}$$

Distributions of the prescribed radiative equilibrium temperature and the relaxation coefficient of temperature are shown in Figure 1. The atmosphere is integrated with no moist processes, no topography, no land-sea contrast and no seasonal or diurnal cycle.

3 The dynamical core of ECHAM5

The ECHAM5 model (Roeckner et al., 2003) employs the spectral transformation method with triangular truncation to solve numerically the governing equations of the atmosphere (Hoskins and Simmons, 1975; Roeckner et al., 2003). The prognostic variables are vorticity, divergence, temperature and the logarithm of the surface pressure. A semi-implicit leapfrog scheme is used to advance in time and the growth of spurious computational modes is inhibited by a weak time filter. In the vertical, a hybrid coordinate system is used which coincide with pure sigma levels near the surface, with pure pressure levels near the model top and transitional hybrid levels in between. In the standard configuration, the uppermost computational level is at 10 hPa with a total of either 19 or 31 levels. A second-order energy and angular momentum conserving scheme is used for finite

differencing in the vertical (Simmons and Burridge, 1981). The horizontal diffusion scheme in the model is in the form of a scale selective hyperviscosity applied to vorticity, divergence and temperature. To avoid spurious wave reflection at the upper boundary, the damping is enhanced in the upper layers by gradually decreasing the order of the hyper-Laplacian operator.

4 Internal variability in the Held-Suarez test case

The Held-Suarez test case, proposed for intercomparison of the dynamical cores of atmospheric models, aims at evaluating the long-term statistical properties of a three-dimensional global circulation. It does not include external forcing such as varying boundary condition or changing solar radiation. The relaxation of temperature to a prescribed radiative equilibrium is on a timescale of 40 days, and the e-folding time for friction is less than 1 day. Thus the statistics calculated over 1000 days, as proposed by Held and Suarez (1994), can be good representatives of the simulated climate state. However, inherent internal variability causes notable fluctuations even in 1000-day averages of the zonal mean zonal wind, for example. A long-term experiment proceeding more than 22000 days (about 60 years) has been conducted with ECHAM5 at the T42L19 resolution, from which seventeen 1000-day periods are extracted. The standard deviation of the time and zonal mean zonal wind is shown in Figure 2, indicating the existence of low-frequency variation.

To investigate this issue in further detail, the EOF (empirical orthogonal functions) analysis is applied to the 22000-day daily data of the zonal mean zonal wind. The first and second EOFs (Figure 3), contributing 23.6% and 22.1% of the total variance, respectively, indicate the meridional shift of the westerly jets, while the third and fourth denote the strengthening and narrowing of the jets. The power spectrum of the first principal component (PC1) is shown in the lower panel of Figure 4, in which three different regimes can be detected. For high frequencies with periods less than about 8 days, the spectrum decays rapidly with increasing frequency. The spectrum is relatively white in the period range from about 8 to 50 days, whereas it grows slowly as the period increases further, indicating a low-frequency variability. The raw time series of PC1 is shown in the upper panel of Figure 4 with the green curve being PC1 itself, and the red and black curves being 121-day and 365-day running averages. Variations at time scales of thousands of days are detectable even by eye. In fact the issue of internally generated low-frequency variability has been address already by several works, for example James and James (1989), James and James (1992), James et al (1994), Müller et al. (2002), among some others. It has been found that the inherently chaotic nature of the flow in a global atmospheric model with idealized heating and friction could lead to variabilities at timescales of several years or longer.

The low-frequency climate fluctuations in the Held-Suarez test case lead to some uncertainty if we want to assess the convergence properties of the solutions in a quantitative way by using only one realization for each resolution. To deal with this problem, Boer and Denis (1997), in another idealized test with similar aim, divided a 1200-day integration into 10 periods of 120 days. 30 days are then discarded in each period and the remaining 90-day subsections are treated as independent realizations for the statistical test. This approach was later adopted by Jablonowski (1998) for carrying out the Held-Suarez test with the GME model. In order to get robust results from the statistical test, it is necessary to evaluate the independency of the realizations obtained in

this way by analyzing the memory of the climate state.

To do this, the long integration with ECHAM5 described above is divided into 90-day periods. By calculating the 90-day-mean zonal mean zonal wind for each grid point in the pressure-latitude cross-section, we get a time series of the means. Then the lag-1 auto-correlation coefficient of this new time series is obtained as a function of the interval (gap) size between each two periods. Figure 5 shows the result at 250 hPa for latitudes between 50°N and 60° N. The statistical significance of the auto-correlation coefficients for all latitudes at 250 hPa is displayed in Figure 6. It is clear in these plots that the 90-day mean is closely auto-correlated in the westerly wind regions when the gap size is small. The correlation becomes weaker as the interval increases. The 90-day subsections are independent only when the gap size is lager than about 150 days. This is the case for all levels in the troposphere, while in the stratosphere near the model top the memory is even longer.

The memory of the climate state has also been analyzed in another way following von Storch and Zwiers (2001). The idea is to estimate the decorrelation time of the 90-day means. This time the long-term integration is subdivided into 90-day periods with no gap in between. Again we calculate the time and zonal mean zonal wind of these subsections and the auto-correlation coefficients of this new time series. The decorrelation time is then estimated by

$$\tau_D = 1 + 2\sum_{k=1}^{M-1}\left(1 - \frac{k}{M}\right)\rho(k)$$

where $\rho(k)$ denotes the auto-correlation coefficient of lag k and M stands for the max lag. The result is shown in Figure 7. Since the time series is the 90-day mean, the unit of the values in this plot is in fact 90 days. For most grid points in the subtropical regions and mid-latitudes, the decorrelation time ranges between 2 and 3, meaning every two to three 90-day periods of the original time series can be considered as an independent realization. The result is consistent with our estimation from the former approach.

Another long-term experiment of the same length is conducted at T85L31 resolution and the same diagnosis performed. For this integration, at least 60 days should be discarded between 90-day periods to ensure the independency of the subsections (plots not shown). Obviously the memory of the time average varies considerably with resolution. From the two integrations above, it would be difficult to make the estimation for all the other resolutions. However, the 30-day interval used by Boer and Denis (1997) is possibly not sufficient to obtain independent realizations for the statistical test. Due to these analyses, we have decided to use the ensemble method in the following experiments with the ECHAM5 model. Details are described in next section.

5 Resolution experiments with ECHAM5

The central goal of this study is to investigate the sensitivity of the ECHAM5 dynamical core to spatial and temporal resolution with the idealized forcing. The questions we are trying to answer are whether the numerical solutions converge and, if so, at which resolution convergence is achieved within a useful tolerance for practical purpose. This section describes in detail the experiments conducted and the methods employed to analyze the results.

5.1 Experimental design

Three groups of experiments are performed with different configurations:

a. Horizontal resolution experiments

The first group is meant to investigate the model's sensitivity to horizontal resolution. Integrations are conducted at resolutions T31, T42, T63, T85 and T106. The L19 vertical resolution of the standard model version is used for all these horizontal resolutions, while L31 is used for T42 onwards. These are in fact the same resolutions as used in Roeckner et al (2006), except that we exclude the lowest (T21L19) and highest (T159L31) resolutions of that study. Default time steps for the full ECHAM5 model are adopted for each resolution (Table 1).

b. Vertical resolution experiments

The second group of integrations is conducted with different vertical resolutions. T85 is chosen as the horizontal grid based on results from the horizontal resolution experiments. Besides the standard L19 and L31 configurations, L46, L61 and L81 grids are also constructed. Location of the uppermost computational level remains the same (namely 10 hPa) for all the resolutions. Other layers of the L31 grid are evenly refined to get higher resolutions. Figure 8 shows the A and B parameters of the vertical coordinate (Roeckner et al. 2003) at resolution L31 and L81. Figure 9 shows the height and thickness of the layers for all five resolutions. Experiments from L31 onwards in this group are integrated with the 480-second time step which is the default value for the standard full ECHAM5 model at T85L31 resolution.

c. Time step experiments

The third group of experiments is integrated at the fixed T85L31 spatial resolution with 4 different times steps: 240, 480, 900 and 1200 seconds. These are meant to investigate the impact of the time step on the solutions.

5.2 Methodology

a. Initialization

The Held-Suarez test focuses on the long-term statistical properties of the simulated global circulation. After integrating for a certain period of time, the prescribed forcing drives the model dynamics to a quasi-equilibrium state that is assumed to be independent of the initial state. One way of initializing the integrations is to use realistic fields or start from an earlier run of the full model. In this case, as long as the inconsistency between the initial fields and the idealized settings of the test case does not lead to computational instability, the climate state can be achieved as already shown by many other models. Another possible way is to start from an isothermal state at rest, in which deviation of the initial temperature from the prescribed radiative equilibrium temperature will lead to the evolution of the general circulation. However, these constant initial fields will not evolve to the expected equilibrium state in spectral models because the spectral discretization and the diffusion scheme are exactly symmetric. Figure 10 depicts the instantaneous field of zonal wind at day 1200 in an integration with ECHAM5 starting from the static state. The results show exact zonal and hemispheric symmetry. Weak easterly wind appears near the surface as well as in a narrow region at the equator in the middle troposphere. Strong

westerly wind extends to model top with core regions located in the low-latitudes. In the absence of wave activity, the temperature distribution (Figure 11) is quite close to the prescribed radiative equilibrium temperature (Figure 1). We have found similar results by repeating this experiment with the NCAR CAM3 model (Collins et al. 2004) (not shown), which indicates that asymmetric perturbations in the initial state are necessary for spectral models to obtain the expected climate state in the Held-Suarez test case, although this may not be true for finite difference models.

b. Ensembles

Based on the analysis in section 4, the ensemble method is employed in our experiments to evaluate the sensitivities of solutions. Since it is computationally expensive to run the model several times for 1200 days at each resolution, and in fact the 100-day statistics are already good representatives of the climate state, we get the ensemble by performing 10 shorter runs. The integrations start from an isothermal state (300K) at rest with random noise added to the spectral coefficients of vorticity and divergence to break the symmetry. For each resolution, the NCAR Command Language random number generator is used to approximate the realization of a large number of independent random variables with a normal distribution. In order to ensure independency, non-overlapping subsections of these random numbers are used to initialize the 10 ensemble runs. Each integration proceeds 300 days. The first 200 days are discarded and the climate state calculated over the third 100 days (The number 100 is chosen rather than 90 or anything else just to facilitate post-processing). Evolution of the temperature variance at 750 hPa in a T85L31 simulation is shown in Figure 12. The model reaches a quasi-equilibrium state after integrating for about 80 days. This is also true at other vertical levels as well as in other simulations with different spatial resolutions and time steps. Therefore by discarding the first 200 days in each integration, we are reasonably certain to have the spin-up period excluded. This approach is not quite efficient in the sense that we "waste" two thirds of every integration. However it is the most convenient way to make sure that the realizations we finally obtain are really independent and not affected by the spin-up process.

   A single realization proceeding 1200 days is also performed for each resolution to produce results that are directly comparable to previous studies with other models following the proposal of Held and Suarez (1994). For ECHAM5, results obtained by these two types of integrations are generally consistent, although with the ensembles we are able to account for the uncertainties induced by the inherent variability in the long-term solutions of the primitive equations.

c. Quantitative evaluation of convergence

Considering the zonally symmetric feature of the forcing terms in the test case, we focus on the zonally averaged climate state in our analyses. Due to the lack of an analytical solution, the highest resolutions in each experiment group are taken as the reference solutions, namely T106L19 and T106L31 for the L19 and L31 simulations in the first group, respectively, T85L81 for the second group and integrations with 240-second time step in the third group. Significance of the differences between the reference resolution and the lower ones is assessed in a statistical way by a local Student's t-test for each grid point, with the t-statistic constructed as

$$T = \frac{\hat{\mu} - \hat{\mu}_r}{\sqrt{(n-1)S^2 + (n_r - 1)S_r^2}} \sqrt{\frac{n \cdot n_r \cdot (n + n_r - 2)}{n + n_r}}$$

Here $\hat{\mu}$ and S are the ensemble mean and ensemble standard deviation of climate state X, given by

$$\hat{\mu} = \frac{1}{n}\sum_{i=1}^{n} X_i \quad \text{and} \quad S = \left[\frac{1}{n-1}\sum_{i=1}^{n}(X_i - \hat{\mu})^2\right]^{\frac{1}{2}}$$

where n is the number of independent realizations ($n=10$ for all the experiments). $\hat{\mu}_r$, S_r and n_r are the corresponding parameters of the reference resolution. Under the hypothesis $\hat{\mu} = \hat{\mu}_r$, the variable T has a Student-t distribution with $n+n_r$-2 degrees of freedom. Difference between $\hat{\mu}$ and $\hat{\mu}_r$ is judged to be significant when the absolute value of the t-statistic exceeds the critical value of a certain significance level (0.01 or 0.05).

Besides the local t-test, we define the following error norm to evaluate the convergence properties at all grid points as a whole:

$$e_1(\hat{\mu}) = \frac{\int_{p_T}^{p_B}\int_{-\pi/2}^{\pi/2}\left|\hat{\mu}(\varphi, p) - \hat{\mu}_r(\varphi, p)\right|\cos\varphi d\varphi dp}{\int_{p_T}^{p_B}\int_{-\pi/2}^{\pi/2}\left|\hat{\mu}_r(\varphi, p)\right|\cos\varphi d\varphi dp}$$

Here φ and p denote the latitude and pressure, respectively, while other notations are the same as defined before. Since the lowest surface pressure in the experiments are around 970 hPa, data on isobaric levels below 970 hPa (p_B) are not included in the calculation to avoid artificial biases due to extrapolation. Layers higher than 200 hPa (p_T) are also ignored to exclude the differences resulting from changes in horizontal diffusion scheme.

It is to be noted that the e_1 error norm is defined following the idea of Williamson et al. (1992) for the shallow water benchmark tests with analytical solutions. However, no analytical solution exists for the Held-Suarez test case in which the long-time statistical properties are the focus. To account for the internal variability of the climate state, another error norm defined as

$$e_s(\hat{\mu}) = \frac{\int_{p_T}^{p_B}\int_{-\pi/2}^{\pi/2}\left|\hat{\mu}(\varphi, p) - \hat{\mu}_r(\varphi, p)\right|\cos\varphi d\varphi dp}{\int_{p_T}^{p_B}\int_{-\pi/2}^{\pi/2} S_r(\varphi, p)\cos\varphi d\varphi dp}$$

is also calculated for each experiment. Other norms appropriate for analyzing convergence of ensemble climate runs are also being investigated.

6 Convergence of the numerical solutions

In this section we compare the responses of the ECHAM5 dynamical core to the idealized forcing at different resolutions by analyzing results of the ensemble experiments. The 1000-day climate will be presented in section 7 for comparison with other models. Basic climate statistics investigated are the time-mean horizontal wind and temperature, eddy temperature variance, eddy kinetic energy, eddy momentum flux and heat flux. These statistics are zonally averaged in addition to the time average as mentioned before.

6.1 Sensitivity to horizontal resolution

a. *Zonal wind*

The latitude-pressure cross sections of zonal-mean zonal wind from five different horizontal resolutions with 19 vertical layers are shown in Figure 13. All resolutions produce similar butterfly-like structures. There is a single westerly jet in each hemisphere maximizing at about 250 hPa, with maximum wind of about 30 ms^{-1}. Easterlies appear in the equatorial and polar lower atmosphere, as well as in the tropics near the model top. These features are in good agreement with those given in Held and Suarez (1994).

Differences between the five different solutions are as follows: Through the whole range of the troposphere, the westerly wind zones shift slightly poleward as the resolution increases. The core regions move a bit downwards and become weaker. The near-surface easterlies in the tropics remain unchanged at all the resolutions, whereas the upper atmosphere band extends and strengthens significantly from T31 to T63. At the lowest resolution (T31), westerly winds prevail at the top layers except for a few grid points in the tropics. The westerly wind decreases with resolution till easterly wind appears near the poles at higher resolutions.

Nevertheless, the results do converge to a certain state when the horizontal grid is fine enough. The wind patterns in T63 and T85 show little difference except for the easterlies near the model top. The patterns of T85 and T106 look almost the same. The indication of convergence is more evidently revealed in Figure 14 by the steady decrease of the differences between the reference solution and the other ones. The differences at T63 are significant only in the tropics and become, in general, statistically insignificant at T85. Features of the L31 simulations are generally quite similar to their L19 counterparts. The decreasing trend of the differences (Figure 15) indicates again convergence of the results.

b. Temperature

The distributions of time and zonal mean temperature at T106L19 resolution is shown in the first panel of Figure 16. Some typical features of the real atmosphere, such as the inversion near the surface in high latitudes and the tropopause structure, are reproduced with the idealized forcing. On the other hand, since the radiative equilibrium temperature is constant in the stratosphere, the Held-Suarez forcing actually keeps the stratosphere inactive, which makes the simulated upper atmosphere unrealistically cold.

Through comparison of the results at different resolutions (Figure 16), it is noticeable that there is gradual warming in middle and high latitudes throughout the atmosphere with the most notable signal occurring in the upper troposphere. Similar changes have been found by Roeckner et al. (2006) in climate simulations with the full ECHAM5 model, especially in the southern hemisphere. Moreover, the pattern of temperature difference between T106L19 and T31L19 in Figure 16 resembles closely the result from the dynamical core experiment with the finite-difference model HadCM3 (Figure 5d in Pope and Stratton 2002). Locations of the strongest warming near the poles are quite similar in these two models although different types of numerical schemes are used for the dynamical cores. This implies that the tropospheric warming in the high latitudes with increased horizontal resolution and the resulting reduction of cold biases, which has been found common in climate simulation with many full models, may be reasonably attributed to the sensitivity of the dynamic core. The convergence of temperature at T85 (Figure 16) is consistent with the full ECHAM5 model (Roeckner et al., 2006). On the other hand, intensified convection at higher horizontal resolutions leads to warming in the tropics in the full

model, while cooling is observed in the idealized test case without moist processes.

c.   Eddy temperature variance

The distributions of the transient eddy temperature variance demonstrate the baroclinic wave activities in the model (Figure 17). As expected, the wave activity is concentrated in the mid-latitude regions. The maximum temperature variance appears in the lower troposphere and extends upward and poleward. A second maximum with smaller magnitude occurs near the tropopause. Increase in horizontal resolution generally leads to enhanced wave activity. The amplitude of temperature variance increases significantly with resolution, due to the ability of the higher resolution versions to resolve smaller scales. Below T85, the core regions of temperature variance move slightly to higher latitudes and rise from the surface to lower model levels. The high resolution simulations show a well-defined maximum near 800 hPa and an indication of convergence can be observed around T85. The L31 simulations show a similar trend (not shown).

d.   Eddy kinetic energy

The transient eddy kinetic energy is another index of baroclinic wave activity. In the pressure-latitude cross section, the single maximum in each hemisphere appears at 250 hPa near 45° latitudes, exactly where the westerly jets reside, while easterlies in the tropics show little variance (the first panel of Figure 18). The magnitude of eddy kinetic energy is quite sensitive to resolution. In both L19 (Figure 18) and L31 (not shown) simulations, it intensifies strongly when horizontal resolution increases. Unlike the other variables mentioned above, the eddy kinetic energy continues to increase when the horizontal resolution goes from T63 to T85. The differences between T85 and T106 are insignificant in the statistical sense.

e.   Eddy fluxes

Eddy heat flux and eddy momentum flux are important mechanisms to establish the general circulation and maintain the energy balance as well as angular momentum conservation of the atmosphere. The simulated zonal mean heat and momentum fluxes at T106L19 resolution and the differences between T106 and other L19 simulations are shown in Figure 19 and Figure 20. The pattern of heat flux is quite similar to that of temperature variance. In most regions, heat is transported poleward, with the strongest flux coinciding with the strongest temperature variance in the middle latitude. The result is heat flux divergence in low latitudes and convergence in the high latitudes. The momentum flux converges in the middle latitudes and maintains the westerly jests there.

   The heat flux enhances significantly with increased horizontal resolution in both L19 and L31 simulations. This is closely related to the strengthening of meridional wind (not shown) and results in the warming in the high latitudes as mentioned before. The momentum flux also enhances with horizontal resolution, but is less sensitive than the heat flux.

f.   Error norms

The e_l and e_s error norms of the climate statistics described above are shown in Figure 21(a,b) and Figure 22(a,b), respectively, indicating the convergence properties of the solutions in a compact way. It is to be noted that for temperature, the magnitude of change with resolution is quite small compared to the characteristic values of the variable itself in unit Kelvin. Consequently the e_l

error norm, denoting the relative error with respect to the reference solution, is two orders smaller than those of the other fields. It has been rescaled for plots in Figure 21 to make the trend visible. The e_s error norm, on the other hand, does not have this normalization problem by using the internal variability of the reference solution as the denominator in the definition. Anyhow the trend of convergence is evident in both senses. The error norms decrease as the horizontal resolution increases and the differences between T85 and T106 simulations are quite small.

6.2 Sensitivity to vertical resolution

Evidence of convergence with increased horizontal resolution has been detected in the former subsections for vertical configurations with 19 and 31 layers, respectively. To see if the L19 and L31 simulations converge to the same state, differences between corresponding simulations are calculated. For T42, increasing the vertical resolution from L19 to L31 doesn't lead to a distinct contrast. However, for higher resolutions, some changes can be detected. The westerly jets shift slightly equatorward when a finer vertical grid is adopted (not shown), which has been found also in the Southern Hemisphere in the full model (Roeckner et al., 2006). For temperature, the independency of difference pattern (L31-L19) on horizontal resolution, as well as the cooling at the tropical tropopause, is also consistent with the full ECHAM5 model (Roeckner et al. 2006). These changes in the full model may be reasonably attributed to the sensitivity of the dynamical core.

In terms of the second-order statistics, finer vertical resolution generally leads to enhancement and equatorward shift of the wave activity (e. g. Figure 23). The changes are more evident in the high-resolution simulations (T85 and T106), which implies the necessity to enhance the vertical and horizontal resolution consistently.

To find out whether the solutions converge when the vertical grid becomes finer, we conduct the group of integrations with various vertical resolutions. The error norms are shown in panel (c) of Figure 21 and Figure 22. Although there is a distinct difference between L19 and L31, characteristics of the simulation do not change significantly when going from L31 to L81. The same trend is true for all the other statistics, according to which we conclude that the numerical solutions do converge as vertical resolution increases. In this idealized test case, 31 layers seem adequate for the horizontal resolution T85 to represent the climate state. In a full GCM, however, convergence will depend on the sensitivity of the employed parameterizations to the vertical resolution.

6.3 Impact of time step

Besides the spatial resolution addressed above, it is also of interest to investigate the model's response to different temporal resolutions and find out if the merit of higher spatial resolution can be achieved by using shorter time steps. This is the motivation for the third group of our experiments with various time steps as described in section 5. Results show that generally the ensemble means do not differ significantly in the statistical sense. Differences between the integration with the shortest time step (240 seconds) and all the other integrations are of the same magnitude as measured by the error norms (panel (d) of Figure 21 and Figure 22). There is no systematic change when the temporal resolution increases. In fact, differences between one

ensemble and the other with immediately shorter or longer time step are often of the opposite sign in the latitude-pressure cross section (Figure 24, panel (a)-(c)). The distributions resemble those of the ensemble standard deviation (Figure 24, panel (d)). Thus it is reasonable to regard these differences as sampling errors and conclude that time step changes within the selected range have little impact on the climate state of this test case.

6.4 Features of the converged solutions

From the analysis above, it has been found that the increase in resolution leads to complicated changes in the features of the simulated climate state. While the second-order statistics tend to enhance with spatial resolution, the strength of the westerly jet increase with horizontal resolution but decrease slightly with vertical resolution. Similarly, core regions of the westerly jet, the eddy temperature variance and kinetic energy shift poleward when the horizontal resolution increases but move equatorward at finer vertical resolution. Therefore it is not easy to find out a single metric to be used as a criterion for "good" solution. Nevertheless some common features are still detectable among the simulations of adequate and consistent resolutions in the ECHAM5 model: The strength of the westerly jet is around 30 m/s with the core regions locating near 42° latitudes. The maxima of transient eddy temperature variance exceed 44 K^2 in the lower troposphere with a well-defined core region located around 40° latitudes. The 40 K^2 contour extends from below 850hPa to a little higher than 700 hPa.

7 Comparison with some other models

The Held-Suarez test case has no analytical solution. Besides investigating the convergence properties of a single model, it is also necessary to compare the results from different models. Since the proposal by Held and Suarez in 1994, this idealized test case has been repeated with many models. The simulated time and zonal mean zonal wind by 6 models is shown in Figure 25. Some properties of these models and simulations are listed in Table 2. Result of ECHAM5 at the comparable resolution (T63L19) is displayed in the first panel of Figure 26, which is calculated by averaging the last 1000 days of a 1200-day integration. In the troposphere, all the models are showing impressively similar pattern even though there are slight differences in the latitudinal location and strength of the westerly jets. In the stratosphere, results vary more evidently. Easterly wind appears in the polar stratosphere in ECHAM5, GME and the finite-volume model of Lin (2004) while westerly wind prevails in the other models. Some models simulate an easterly wind band enhancing with altitude in the tropical stratospheric region, while the GEOS GCM and ECHAM5 present a closed cell near the tropopause. These differences possibly result from the different upper boundary conditions adopted by these models.

Some other 1000-day statistics of ECHAM5 at T63L19 resolution are also shown in Figure 26, together with corresponding plots of the GME model (ni=32) (Figure 27, from Jablonowski 1998) and of the finite-volume model of Lin (2004) at 2°x2.5° resolution (Figure 28, from Lin 2004). The horizontal wind and eddy transport terms simulated by the 3 models are quite similar in terms of both patterns and magnitudes. The eddy kinetic energy in ECHAM5 is significantly larger than in GME. While the maxima in the former exceed 400 m^2s^{-2}, the values are about 280 m^2s^{-2} in the latter. The climate states shown in Figure 27 are averages of the values calculated over ten 90-day

periods. However, according to our experiments with ECHAM5, these statistics obtained from a 100-day period and a 1000-day one are of comparable magnitudes. Thus the difference between ECHAM5 and GME are most likely due to different properties of the numerical schemes rather than the different ways of diagnosis. The bottom-left panel of Figure 28 displays the eddy variance of the zonal wind rather than the kinetic energy. The maxima are about 220 m^2s^{-2} which are also a bit weaker than in ECHAM5 (about 300 m^2s^{-2}, not shown). Similarly, the eddy temperature variance is strongest in ECHAM5 and weakest in GME. In fact the eddy variances in GME at ni=48 resolution (approximately 1.3° at the equator), namely 360 m^2s^{-2} for kinetic energy and 42 K^2 for temperature variance, are closer to those in the other two models at T63 and 2°x2.5°, respectively.

As for the sensitivity to spatial resolution, we have noticed a poleward shift of the westerly jet with increased horizontal resolution in the ECHAM5 model. The same trend has been reported by Fox-Rabinovitz et al. (1997) with a stretched grid model as well as by Jablonowski (1998) with the geodesic grid model GME. In the HadAM3 model (Pope and Stratton, 2002), the westerly jets do not move polewards, but the polar warming at higher resolution with pronounced signal near 200 hPa is quite similar to ECHAM5 and the finite-volume model of Lin (2004). The enhanced baroclinic wave activity, as indicated by increased eddy kinetic energy, temperature variance and flux terms, is a common feature in many models.

8 Summary and concluding remarks

In this study, the test case proposed by Held and Suarez (1994) is performed to test the spectral dynamical core of the ECHAM5 model in the standard version. From a long-term integration at medium resolution (T42L19), it is found that the internal variability of this idealized test case leads to low-frequency variations at time scales as long as thousands of days. The spectrum of the first principal component of the zonal mean zonal wind shows a 3-regime feature: It increases rapidly with period in the high-frequency part, becomes relatively white in the period-range from about 8 to 50 days, and grows again with period in the low-frequency part. The memory of climate state is also investigated and found to vary considerably with horizontal resolution.

The 1200-day simulations as proposed by Held and Suarez (1994) are carried out. As a whole, the climate state simulated by the dynamical core of ECHAM5 with this idealized forcing is comparable to results given by many other global atmospheric general circulation models (e.g. Jablonowski 1998, Ringler et al. 2000 and Lin 2004, among many others). This is true for both the zonal mean states and the baroclinic wave activities in the model. Some differences are also detected, for example the slight differences in the location and strength of the westerly jets and responses near the upper boundary. It is also found that the eddy temperature variance and kinetic energy are stronger in ECHAM5 than in the finite difference model GME (Jablonowski 1998) and the finite volume model of Lin (2004) at the comparable resolution.

Ensemble experiments are conducted with different horizontal and vertical resolutions as well as time steps to assess the sensitivity and convergence of the solutions with ECHAM5. The simulated climate is found to be sensitive to horizontal resolution. In both L19 and L31 simulations, when the grid gets finer, westerly jets in the middle latitudes slightly decrease in strength and shift poleward. Easterlies in the equatorial regions near model top become stronger.

The meridional wind is also enhanced and temperature increases gradually in the high latitudes. Baroclinic wave activities steadily intensify with increased resolution since the additional smaller scales can contribute to the field. Magnitudes of the transient eddy temperature variance and eddy kinetic energy increase strongly at high resolutions compared to the lower ones.

Nevertheless, results of various resolutions seem to converge practically at T85. For the time and zonal mean states investigated, the differences between T63 and T106 are already small. Although the eddy kinetic energy still shows considerable changes when the horizontal resolution goes from T63 to T85, the differences between T85 and T106 are judged to be not significant by the statistical test. The trend of convergence to a certain solution occurs in both L19 and L31 integrations.

It has been found that the solutions are also sensitive to vertical resolution. In fact the aforementioned L19 and L31 simulations converge to different states. Increase of vertical resolution from L19 to L31 leads to even stronger eddy variances and equatorward shift of the westerly jets. The differences are more evident in simulations with high horizontal resolution (T85, T106). A group of integrations at T85 combined with a range of vertical resolutions show that features of the simulation do not change much when the total number of vertical layers exceeds 31. L31 seems adequate for simulating the climate state with this idealized forcing.

Experiments also indicate that time steps within the selected range have little impact on the simulated climate in absence of realistic parameterizations for physics processes. Differences between integrations with various time steps are not larger than the noise level induced by the inherent variability of this test case, and thus can be considered as sampling errors. From all the experiments mentioned above, we come to the conclusion that convergence of numerical solutions by the dynamical core of ECHAM5 has been detected in the Held-Suarez test case. Results at the T85L31 with 1200-second time step can be considered as an adequately good reference solution.

It is worth noticing that some common features have been observed in the idealized test case with the dynamical core and the climate simulations with the full ECHAM5 model. In Roeckner et al. (2006), no evidence for convergence to a more realistic climate state was found at L19 resolution for simulations at horizontal resolutions higher than T42, while for the L31 simulations the errors relative to observations decrease monotonously wither increasing horizontal resolution. Experiments in this study indicate that this is not only due to the dependency of parameterizations schemes on the resolved scales of the model. Actually even for the dynamical core with the prescribed "perfect" forcing, L19 is not enough for horizontal resolutions higher than T42. This conclusion is in accord with those of some earlier studies (Lindzen and Fox-Rabinovitz 1989, Fox-Rabinovitz and Lindzen 1993) implying that horizontal and vertical resolution should be chosen consistently.

Moreover, such phenomena as polar warming in high latitudes at increased horizontal resolution and equatorward shift of the westerly jet with finer vertical grid imply that some changes occurring in the full model can be directly attributed to the sensitivity of the dynamical part to spatial resolution. This, to some extent, gives us useful hints on the tuning of parameterization schemes when more realistic climate simulations are expected with higher resolution.

References

Boer, G. J. and B. Denis (1997): Numerical convergence of the dynamics of a GCM. Clim. Dyn. 13, 359-374

Boyle, J. (1993): Sensitivity of dynamical quantities to horizontal resolution for a climate simulation using the ECMWF (Cycle 33) model. J. Clim., 6, 796-815

Chen, M., J. R. Bates (1996): A comparison of climate simulations from a semi-Lagrangian and an Eulerian GCM. J. Clim. 9, 1126-1148

Chen, M., R. B. Rood and L. L. Takacs (1997): Impact of a semi-Lagrangian and an Eulerian dynamical core on climate simulation. J. Clim. 10, 2374-2389

Collins, W. D. et al. (2004): Description of the NCAR community atmosphere model (CAM3.0). NCAR Technical Note NCAR/TN-464+STR. National Center for Atmospheric Research, Boulder, Colorado, 226 pp.

Fox-Rabinovitz, M.S. and R.S. Lindzen (1993): Numerical experiments on consistent horizontal and vertical resolution for atmospheric models and observing systems. Mon. Wea. Rev., 121, 264-271.

Fox Rabinowitz et al., (1997): A finite difference GCM dynamical core with variable resolution stretched grid, Mon. Wea. Rev., 125, 2943-2968

Held, I. M. and M. J. Suarez, (1994): A proposal for the intercomparison of the dynamical cores of atmospheric general circulation models, Bull. Amer. Meteor. Soc., 75: 1825-1830.

Hoskins, B. J. and Simmons, A. J. (1975): A multi-layer spectral model and the semi-implicit method. Quart. J. Roy. Meteor. Soc., 101, 637-655.

Lin S.-J. (2004): A ''Vertically Lagrangian'' Finite-Volume Dynamical Core for Global Models. Mon. Wea. Rev., 132, 2293-2307

Lindzen, R.S. and M.S. Fox-Rabinovitz (1989): Consistent vertical and horizontal resolution. Mon. Wea. Rev., 117, 2575-2583.

Jablonowski, C. (1998): Test der Dynamik zweier globaler Wettervorhersagemodelle des Deutschen Wetterdienstes: Der Held-Suarez Test. Diplomarbeit, 140pp.

James I. N. and P. M. James (1989): Ultra-low-frequency variability in a simple atmospheric circulation model. Nature 342, 53-55

James I. N. and P. M. James (1992): Spatial structure of ultra-low-frequency variability of the flow in a simple atmospheric circulation model. Quart. J. Roy. Meteor. Soc. 118, 1211-1233

James P. M., K. Fraedrich and I. N. James (1994): Wave-zonal-flow interaction and ultra-low-frequency variability in a simplified global circulation model. Quart. J. Roy. Meteor. Soc. 120, 1045-1067

Müller, W., R. Blender and K. Fraedrich (2002): Low-frequency variability in idealized GCM experiments with circumpolar and localized storm tracks. Nonlinear Process Geophys. 9, 37-49

Phillips T. J., L. C. Corsetti, S. L. Grotch (1995): The impact of horizontal resolution on moist processes in the ECMWF model. Clim. Dyn. 11, 85-102

Pope V. D., J. A. Pamment, D. R. Jackson, A. Slingo (2001): The representation of water vapour and its dependence on vertical resolution in the Hadley Centre climate model. J. Clim. 14, 3065-3085

Pope V. D. and R. A. Stratton, (2002): The processes governing horizontal resolution sensitivity in a climate model. Clim. Dyn. 19, 211-236

Ringler, T. D., R. P. Heikes, and D. A. Randall (2000): Modeling the atmospheric general circulation using a spherical geodesic grid: a new class of dynamical cores. Mon. Wea. Rev., 128: 2471-2490.

Roeckner, E., et al. (2003): The atmospheric general circulation model ECHAM5. Part I: Model description. Rep. No. 349, Max Planck Institut for Meteorology, Hamburg, Germany. 127pp.

Roeckner, E. et al. (2006): Sensitivity of simulated climate to horizontal and vertical resolution. J. Clim. (accepted)

Simmons, A.J. and D.M. Burridge (1981): An energy and angular-momentum conserving vertical finite difference scheme and hybrid vertical coordinates. Mon. Wea. Rev., 109, 758-766.

Stratton, R. A. (1999): A high resolution AMIP integration using the Hadley Centre model HadAM2b. Clim. Dyn. 15, 9-28

University Corporation for Atmospheric Research: NCAR Command Language. http://ngwww.ucar.edu/ncl/

von Storch H. and F. W. Zwiers (2001): Statistical analysis in climate research. Chapter 6: The statistical test of a hypothesis. Cambridge University Press.

Williamson, D. L., et at. (1992): A standard test set for numerical approximations to the shallow water equations in spherical geometry. J. Comput. Phys. 102, 211-224

Williamson, D. L., J. T. Kiehl, J. J. Hack (1995): Climate sensitivity of the NCAR community climate model (CCM2) to horizontal resolution. Clim. Dyn. 11, 377-397

Williamson D. L., J. G. Olson, B. A Boville. (1998): A comparison of semi-Lagrangian and Eulerian tropical climate simulations. Mon. Wea. Rev. 126, 1001-1012

Resolution	T31L19	T42L19	T63L19	T85L19	T106L19
Time Step (second)	2400	1800	1200	900	720
Resolution		T42L31	T63L31	T85L31	T106L31
Time Step (second)		1200	720	480	360

Table 1   Default time step (in seconds) of the full ECHAM5 model at various resolutions.

Panel in Figure 25	a	b	c	d	e	f
Model type	Spectral	Finite difference	Finite difference	Finite difference	Finite volume	Finite difference
Horizontal grid	Gaussian grid	Latitude-longitude grid	Spherical icosahedral grid	Spherical icosahedral grid	Latitude-longitude grid	Latitude-longitude grid
Horizontal resolution	T63 (1.87°)	2° latitude 2.5° longitude	Ni=32 (approx. 2° at the equator)	10242 grid cells (approx. 2.16° at the equator)	2° latitude 2.5° longitude	2° latitude 2.5° longitude
Vertical grid	20 σ levels	20 σ levels	19 hybrid p-σ levels	17 σ levels	32 hybrid p-σ levels	20 σ levels
Length of integration for calculating climate state	1000 days	1000 days	90 days (10 periods in total)	450 days	1000 days	1000 days
Westerly jet strength	> 28 m/s	> 28 m/s	> 30 m/s	> 32 m/s	> 32 m/s	> 30 m/s

Table 2   Properties of the models and simulations in Figure 25
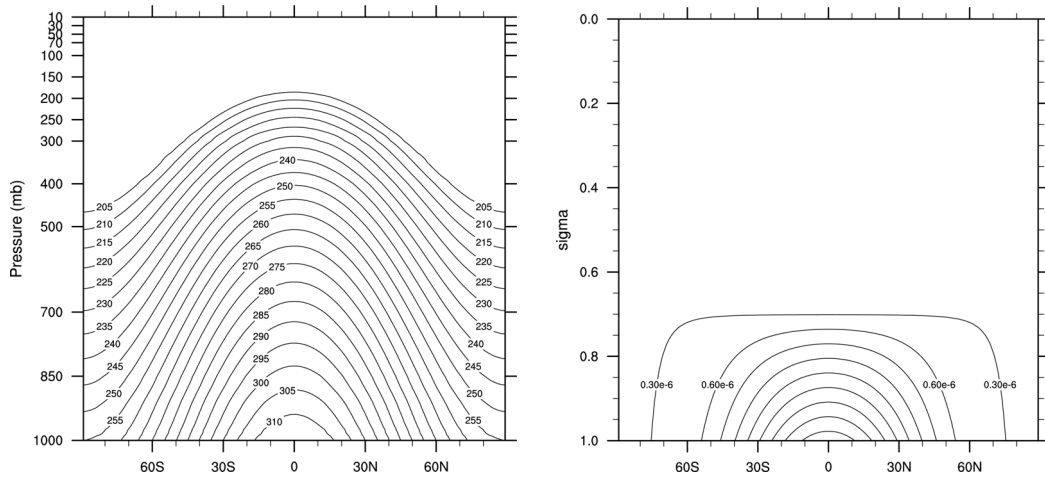
Figure 1   The prescribed radiative equilibrium temperature (left. Unit: K) and relaxation coefficients of temperature (right) in the Held-Suarez test case. Contour intervals are 5 K and 3e-6, respectively.
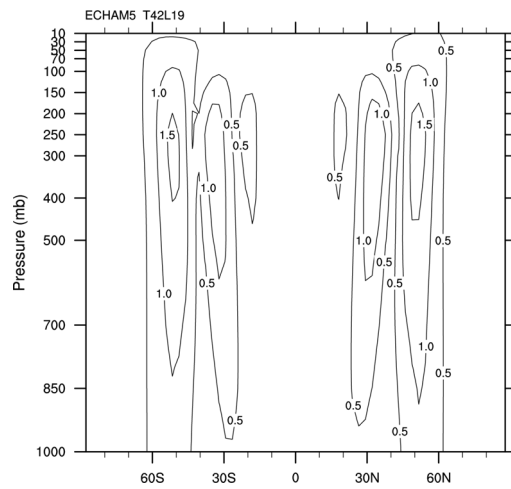
Figure 2   Standard deviation of the 1000-day mean zonal mean zonal wind (ms^{-1}) in a long-term integration with ECHAM5 at T42L19 resolution. Contour interval is 0.5 ms^{-1}.
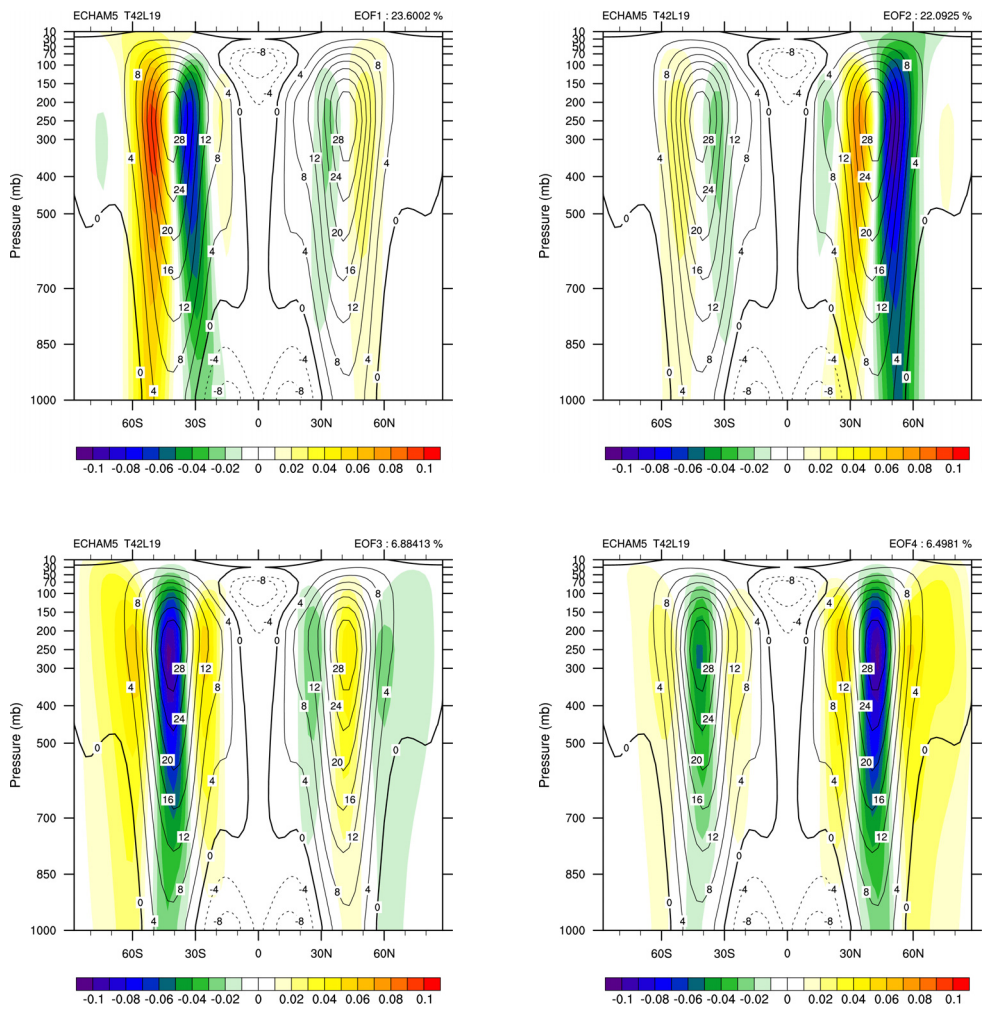
Figure 3   The time and zonal mean zonal wind (black contours. The interval is 4 ms^{-1}) and
the first 4 EOFs (color shading) of the zonal mean zonal wind in a long-term
integration with ECHAM5 at T42L19 resolution.
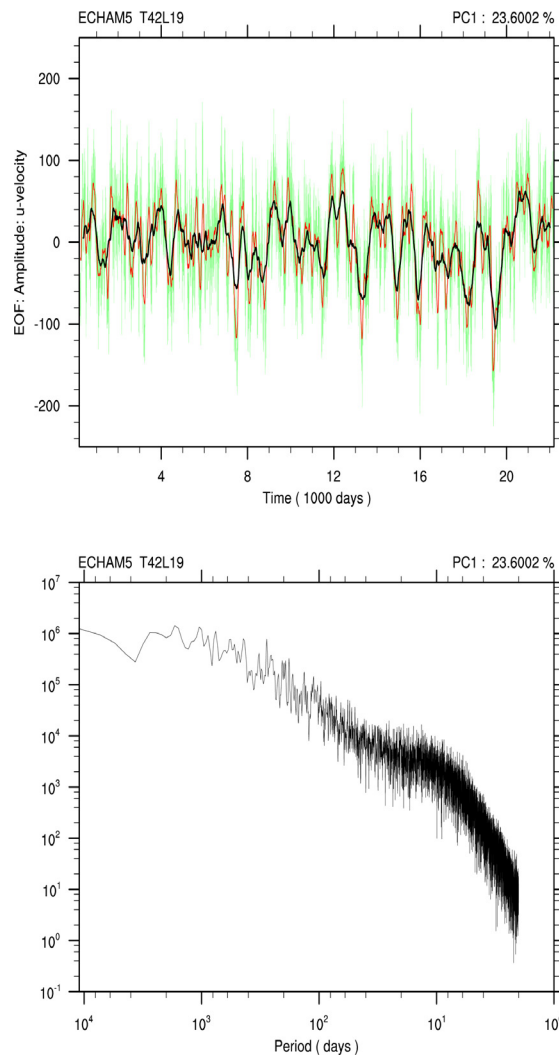
Figure 4   top: The time series of the amplitude of the first EOF in Figure 3 (green curve) and
the 121-day (red) and 365-day (black) running averages.
bottom: The power spectra of the time series.
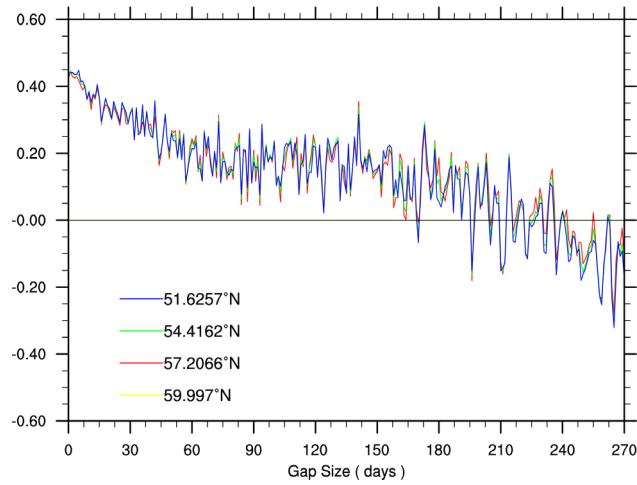
Figure 5   Lag-1 auto-correlation coefficient of the time series of 90-day-mean zonal-mean
zonal wind as a function of gap sized between each two periods. Shown in this
plots are results at 250 hPa between 50°N and 60°N in a long-term integration
with ECHAM5 at T42L19 resolution.
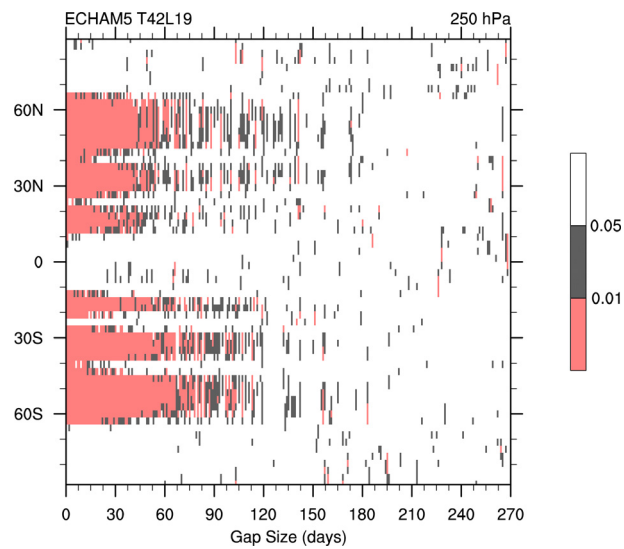
Figure 6   Statistical significance of the lag-1 auto-correlation coefficient of the time series of
90-day-mean zonal-mean zonal wind in a long-term integration with ECHAM5 at
T42L19 resolution
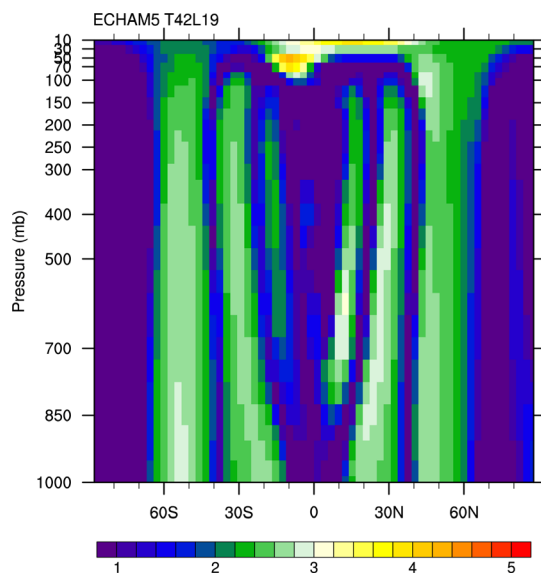
Figure 7   The estimated decorrelation time in case of taking 90-periods without gap in between as independent realizations. The unit is 90 days.
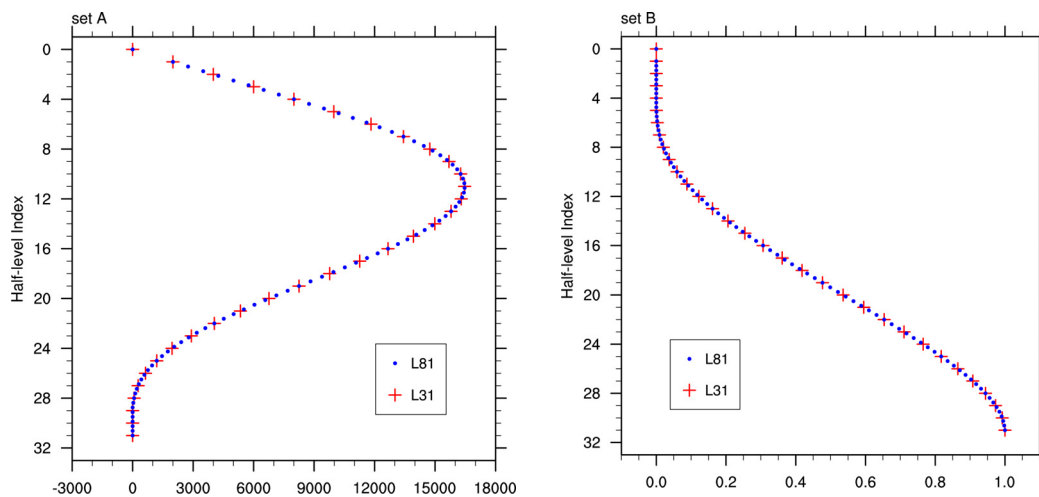
Figure 8   The vertical coordinate parameters A (left) and B (right) at L31 and L81 resolutions. Level indices increase from model top to the earth's surface. The L81 indices are scaled to the L31 index range.
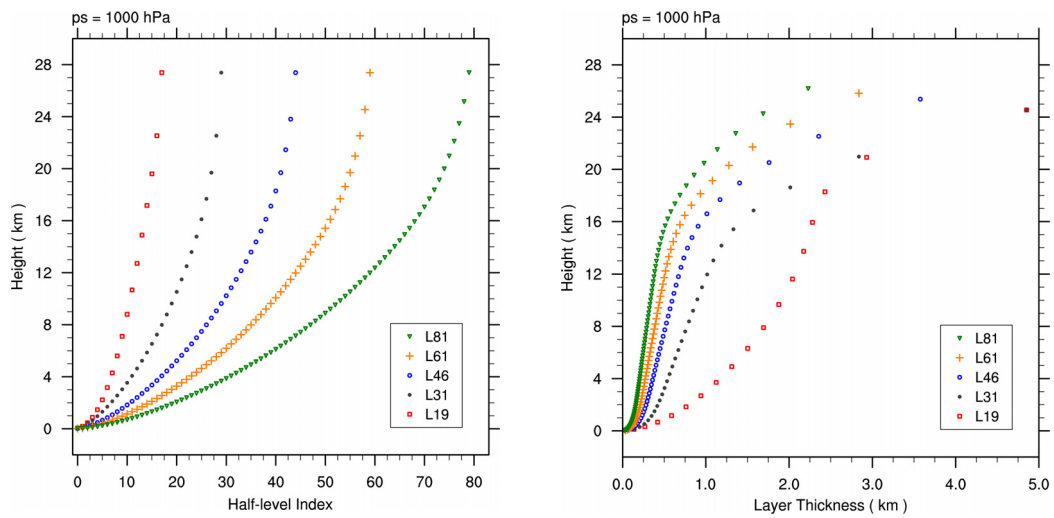
Figure 9   The height (left) and thickness (right) of model layers at different vertical resolutions. Level indices in the left panel increase from the earth's surface to model top.
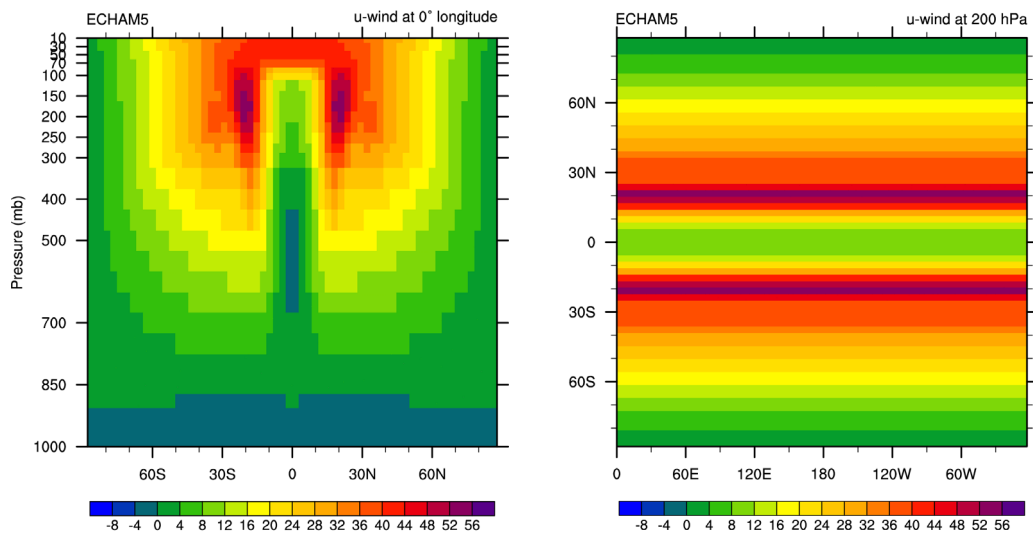
Figure 10   Snapshot of the zonal wind (ms⁻¹) at day 1200 in the simulation starting from an isothermal static state. Left: pressure-latitude cross-section at 0° longitude. Right: geographical distribution at 200 hPa.
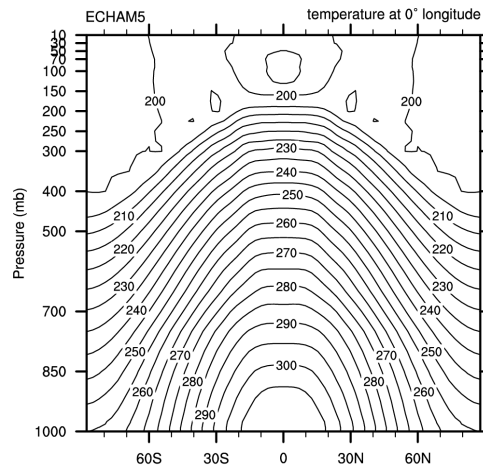
Figure 11   Snapshot of temperature (K) at day 1200 in the simulation starting from an isothermal static state.
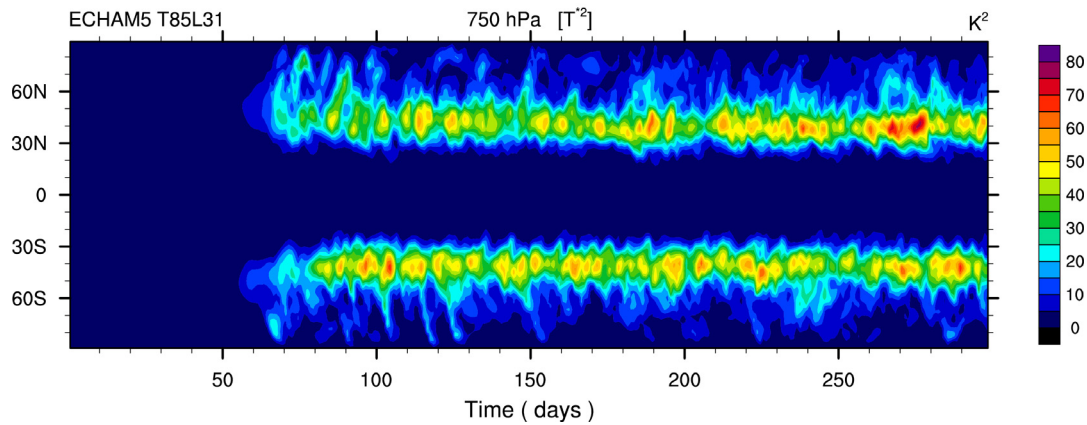
Figure 12   Evolution of 750hPa temperature variance in the first 300 days in one integration with ECHAM5 at T85L31 resolution.
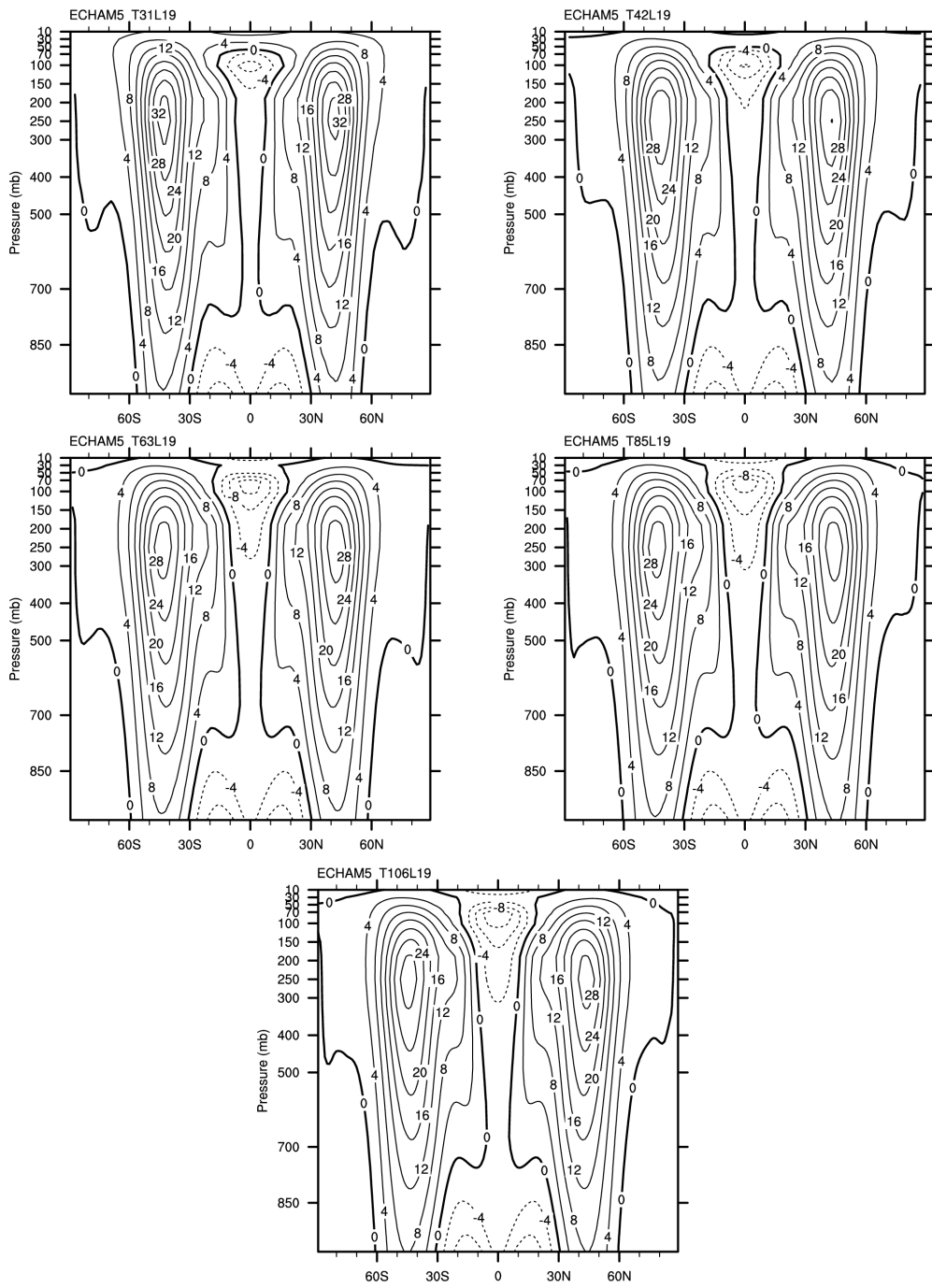
Figure 13   Zonal-mean zonal wind (ms^{-1}) in L19 simulations of ECHAM5 at different horizontal resolutions. Contour interval is 4 ms^{-1}.
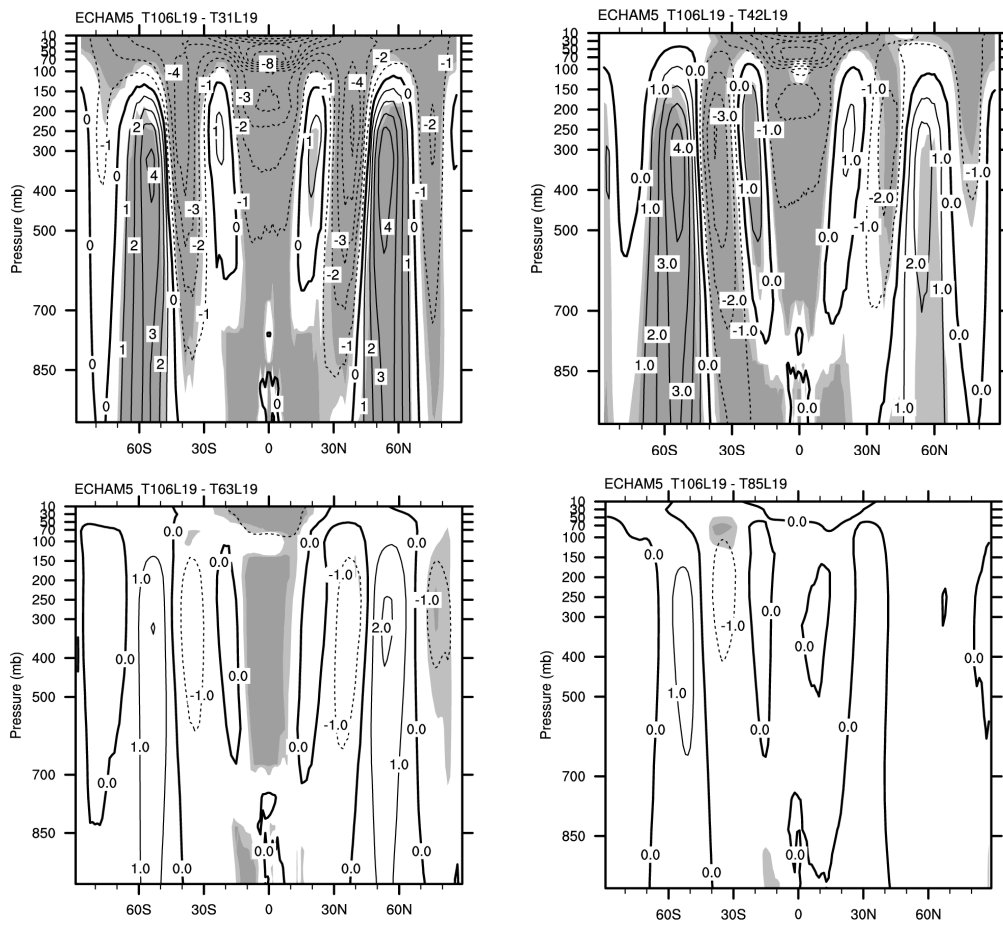
Figure 14 Zonal-mean zonal wind differences (ms^{-1}) between T106L19 and other L19 simulations. Contour interval is 1 ms^{-1}. Light and dark shaded areas are judged to be significantly different by the local t-test at 0.05 and 0.01 significance levels, respectively.
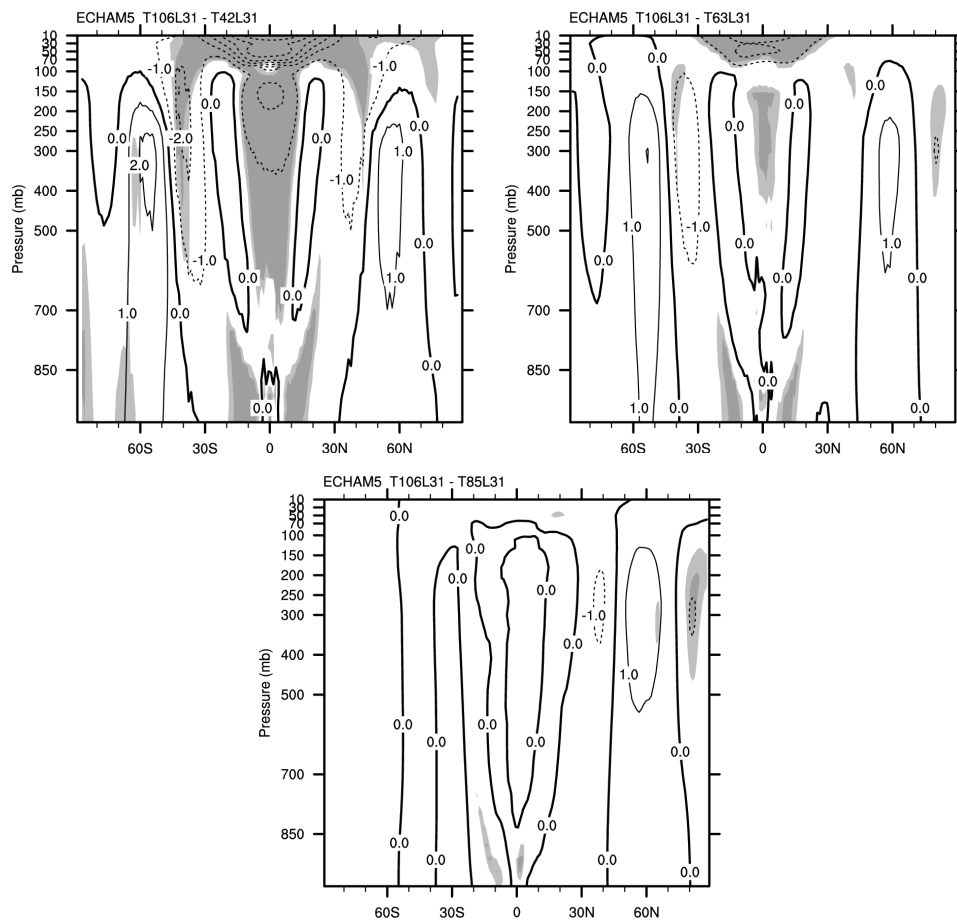
Figure 15   Zonal-mean zonal wind difference (ms^{-1}) between T106L31 and other L31 simulations. Contour interval is 1 ms^{-1}. Light and dark shaded areas are judged to be significantly different by the local t-test at 0.05 and 0.01 significance levels, respectively.
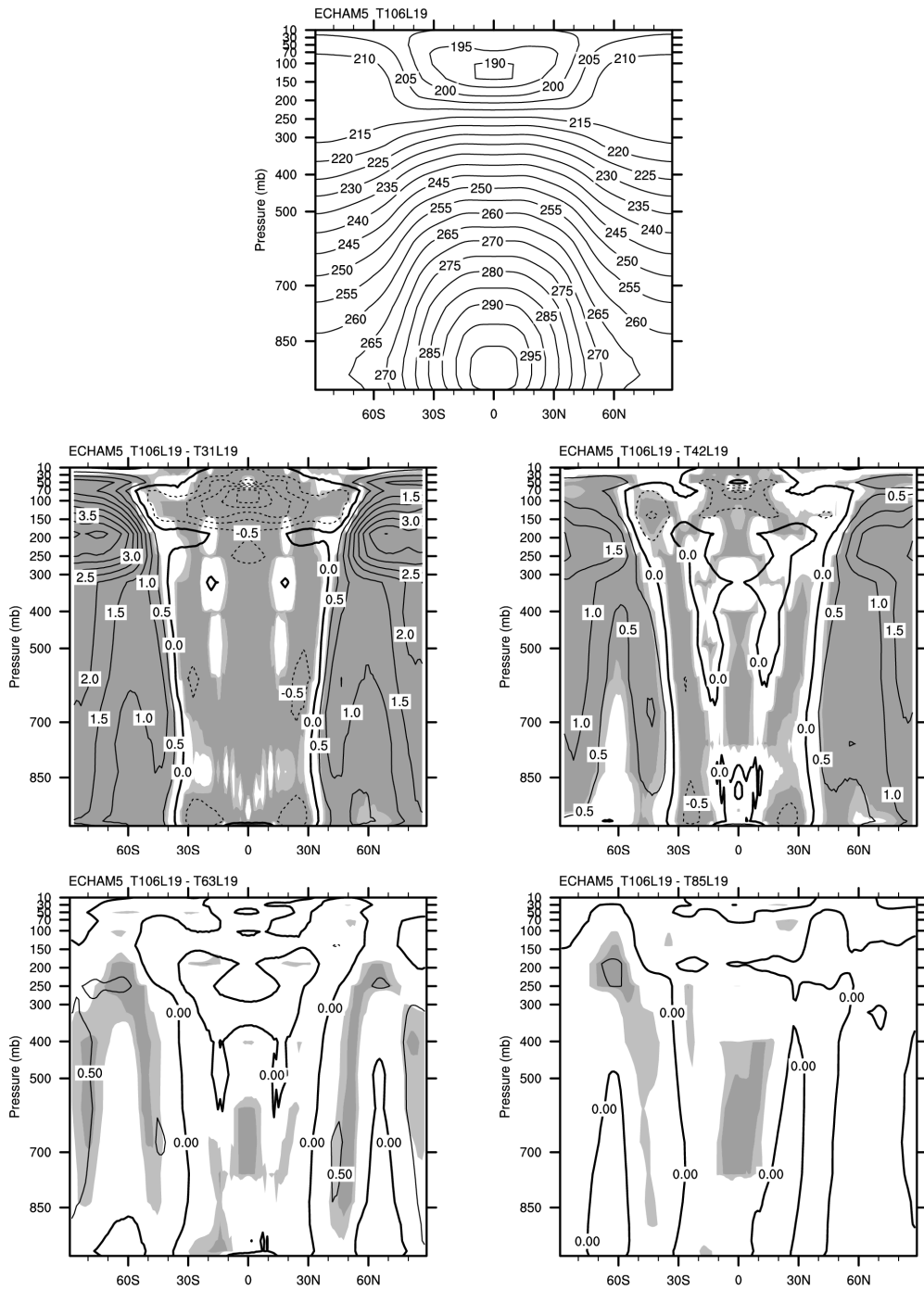
Figure 16   Zonal-mean temperature (K) simulated by T106L19 (top center) and the differences between T106 and other L19 simulations. Contour interval is 5 K in the first panel and 0.5 K in the other ones. Light and dark shaded areas are judged to be significantly different by the local t-test at 0.05 and 0.01 significance levels, respectively.
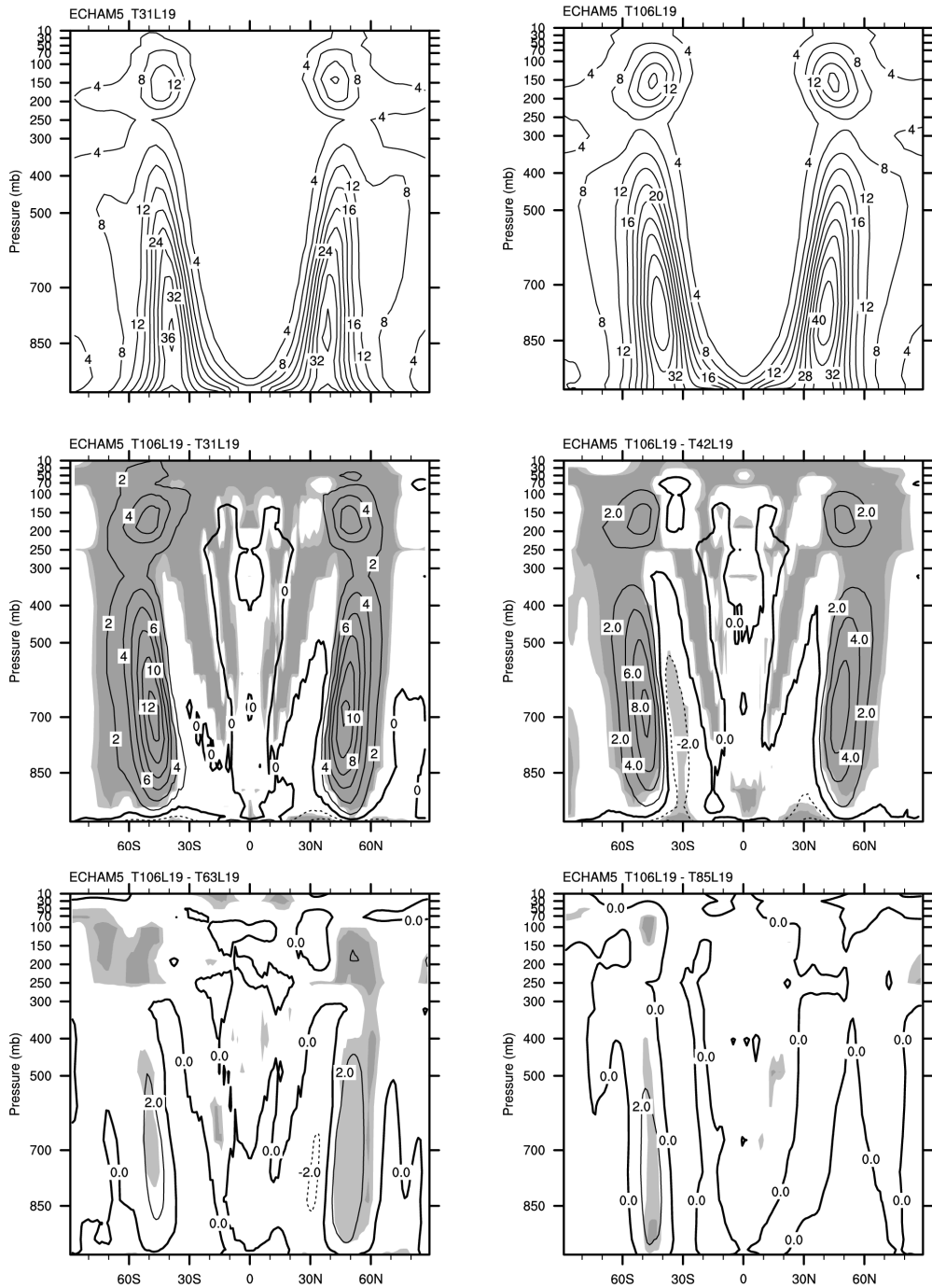
Figure 17   Zonal-mean eddy temperature variance given by T31L19 (top left) and T106L19 (top right), and the differences between T106 and other L19 simulations. Contour interval is 4 K^2 in the first two panels and 2 K^2 in the other ones. Light and dark shaded areas in the last 4 panels are judged to be significantly different by the local t-test at 0.05 and 0.01 significance levels, respectively.
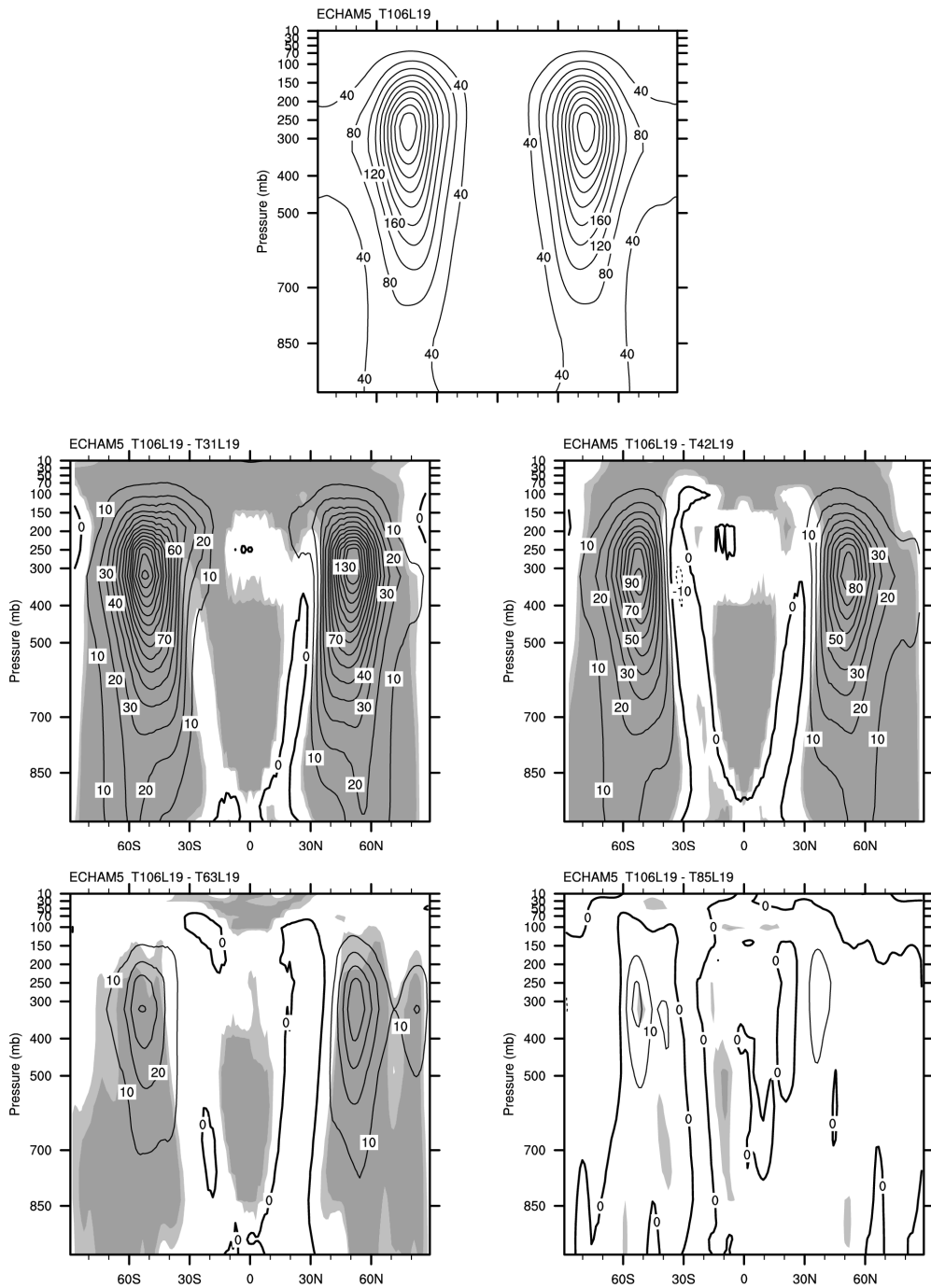
Figure 18   Zonal-mean eddy kinetic energy given by T106L19 (top center), and the differences between T106 and other L19 simulations. Contour interval is 40 m^2s^{-2} in the first panel and 10 m^2s^{-2} in the other ones. Light and dark shaded areas in the last 4 panels are judged to be significantly different by the local t-test at 0.05 and 0.01 significance levels, respectively.
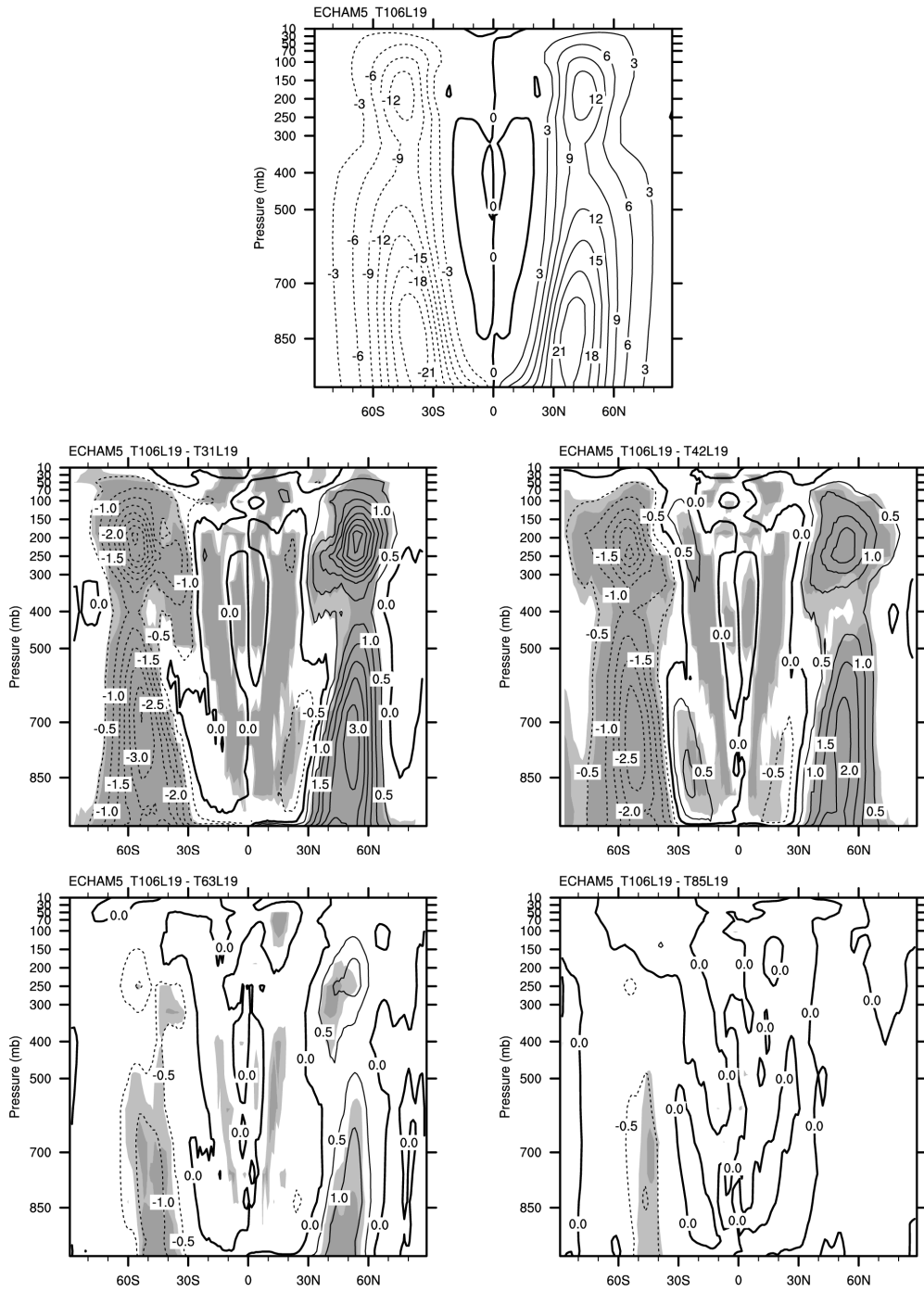
Figure 19   Zonal-mean eddy heat flux given by T106L19 (top center), and the differences between T106 and other L19 simulations. Contour interval is 3 Kms⁻¹ in the first panel and 0.5 Kms⁻¹ in the other ones. Light and dark shaded areas in the last 4 panels are judged to be significantly different by the local t-test at 0.05 and 0.01 significance levels, respectively.
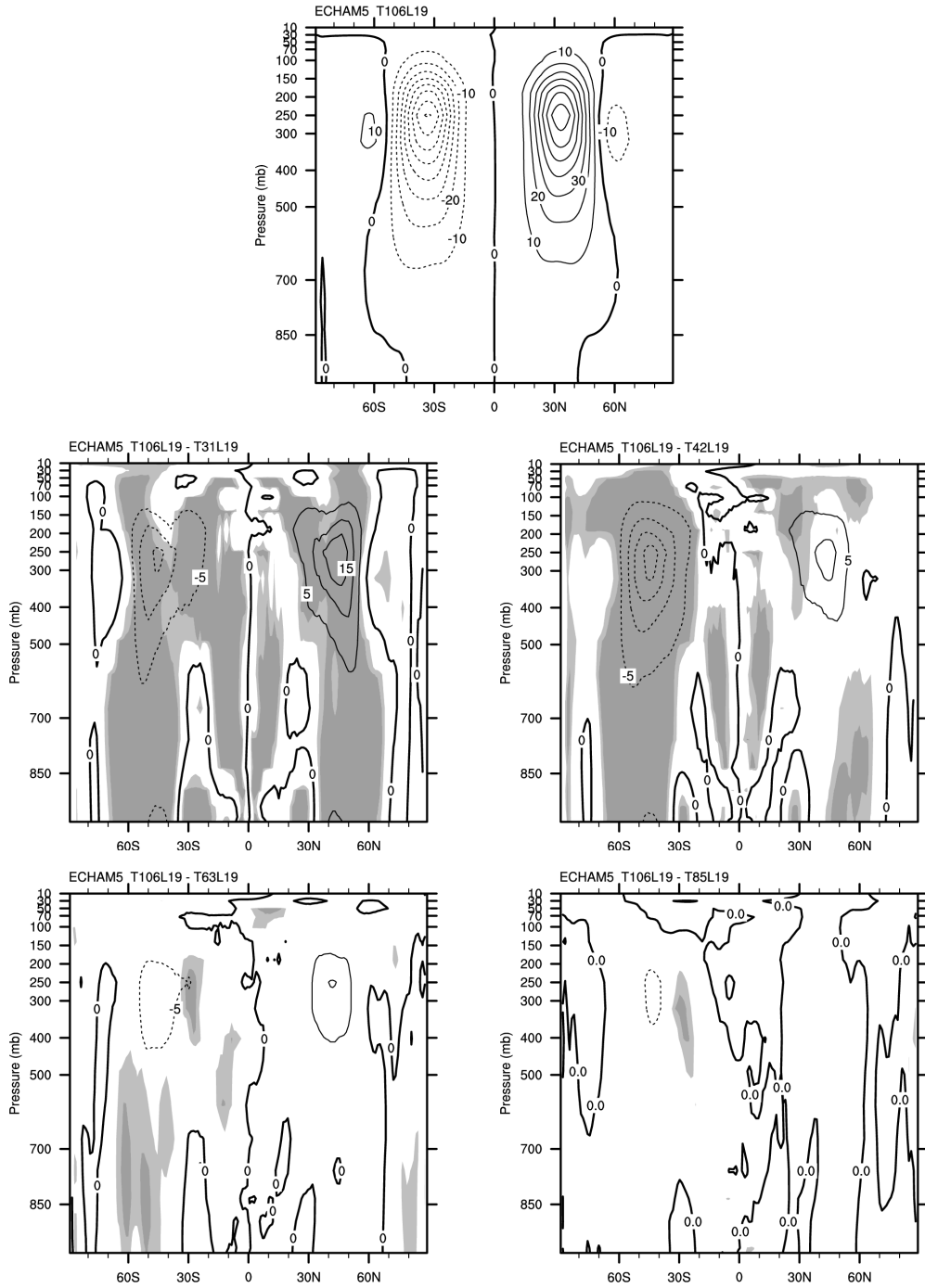
Figure 20   Zonal-mean eddy momentum flux given by T106L19 (top left), and the
differences between T106 and other L19 simulations. Contour interval is 10 m^2s^{-2}
in the first panel and 5 m^2s^{-2} in the other ones. Light and dark shaded areas in the
last 4 panels are judged to be significantly different by the local t-test at 0.05 and
0.01 significance levels, respectively.
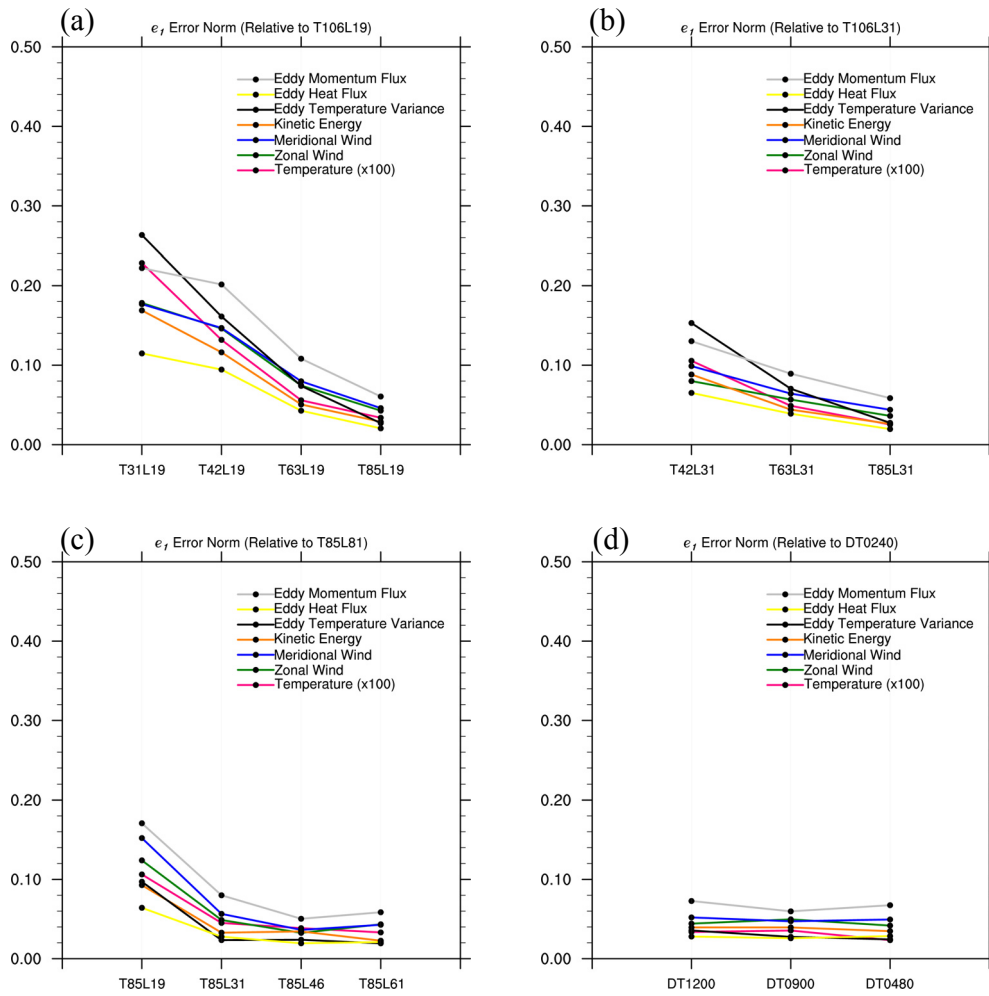
Figure 21　The e_1 error norm relative to the reference solution in
　　　　　(a) and (b): horizontal resolution experiments;
　　　　　(c): vertical resolution experiments;
　　　　　(d): time step experiments.
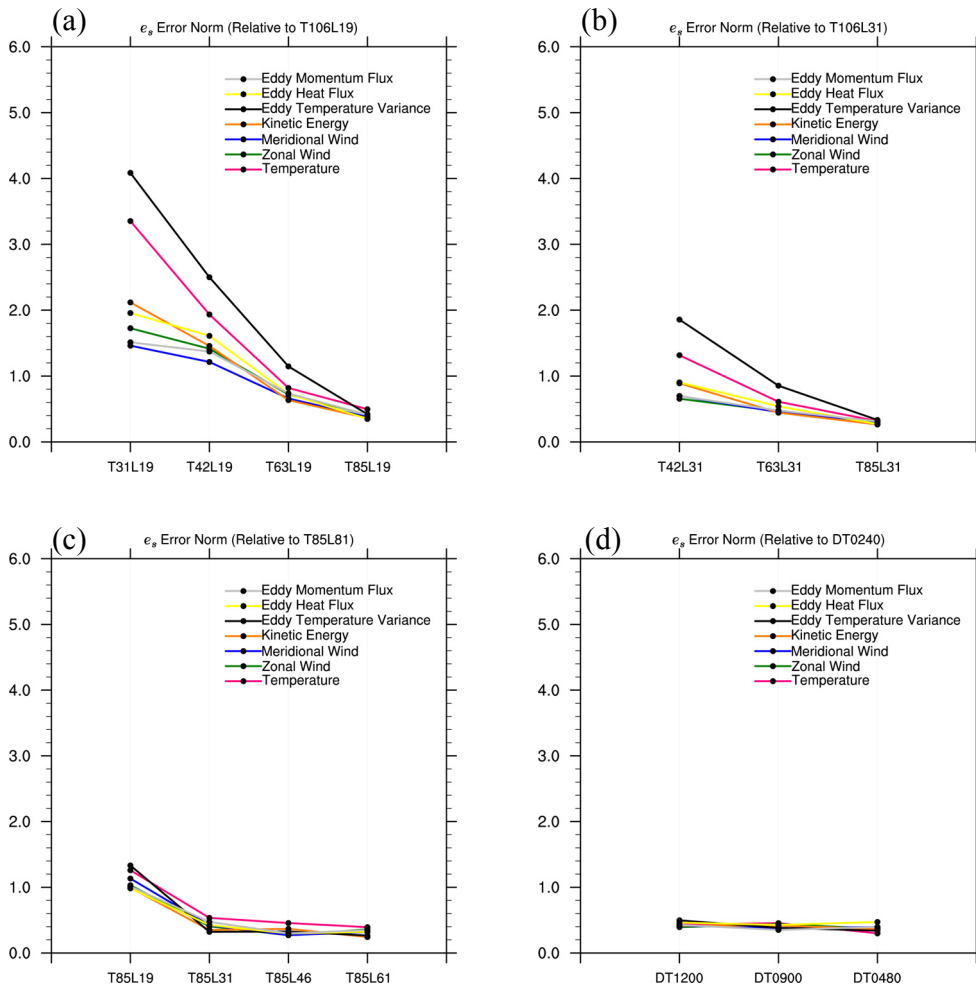
Figure 22　The e_s error norm relative to the reference solution in
(a) and (b): horizontal resolution experiments;
(c): vertical resolution experiments;
(d): time step experiments.
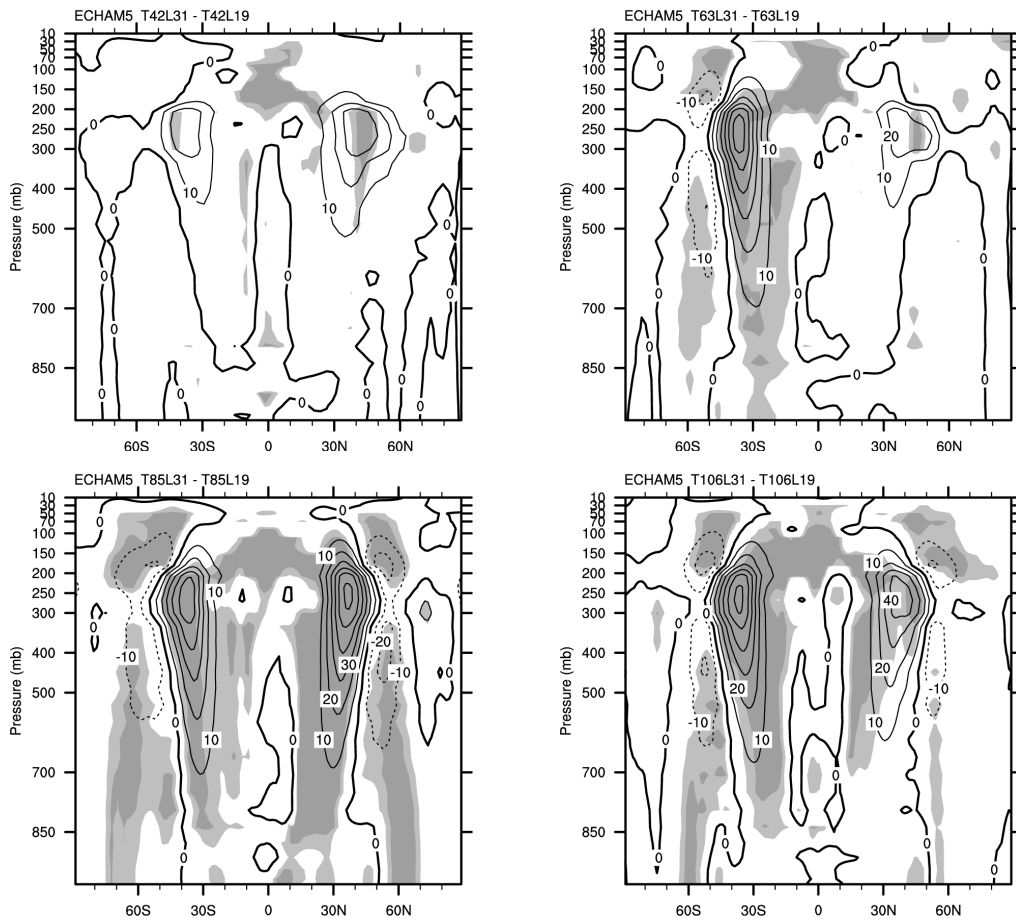
Figure 23   Difference of zonal-mean eddy kinetic energy between L31 and L19 simulations for horizontal resolutions T42, T63, T85 and T106. Contour interval is 10 $m^2 s^{-2}$. Light and dark shaded areas are judged to be significantly different by the local t-test at 0.05 and 0.01 significance levels, respectively.
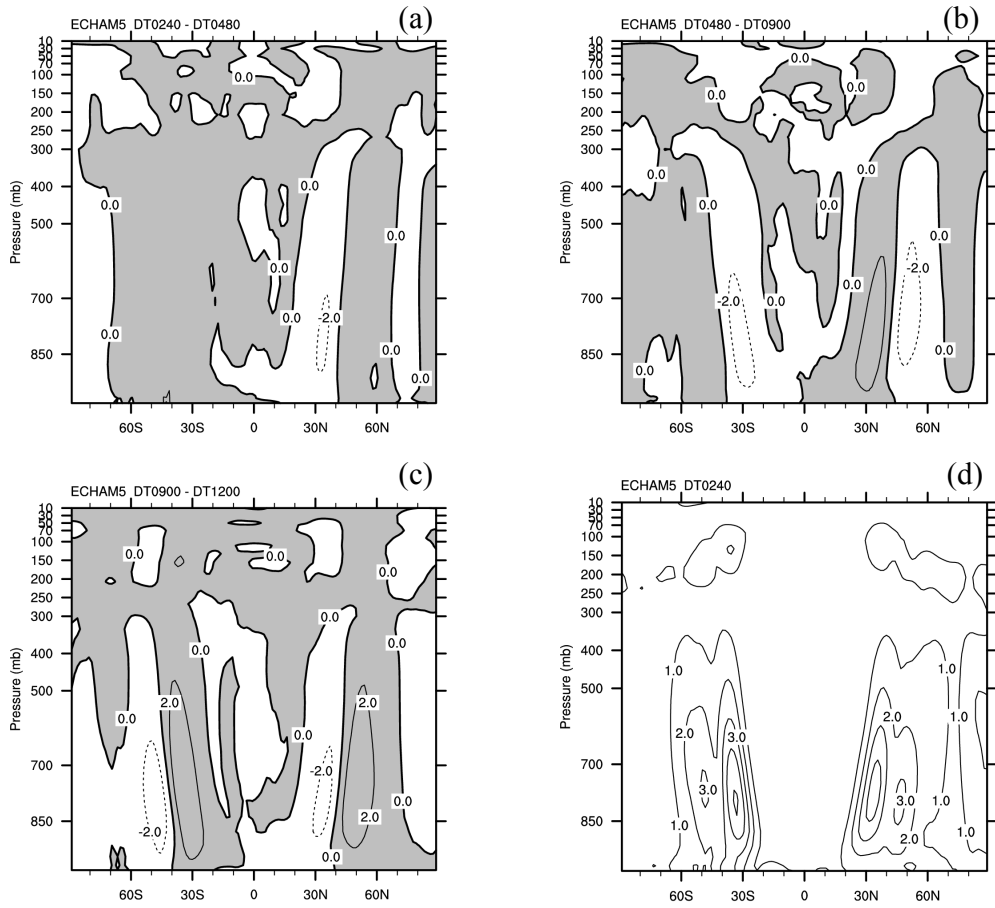
Figure 24   (a)-(c): Differences of zonal-mean eddy temperature variance (K^2) between integrations with same spatial resolution (T85L31) and different times step sizes. Contour interval is 2 K^2 with positive values shaded. (d) Ensemble standard deviation of the eddy temperature variance (K^2) for the integrations with 240-second time step. Contour interval is 1 K^2.
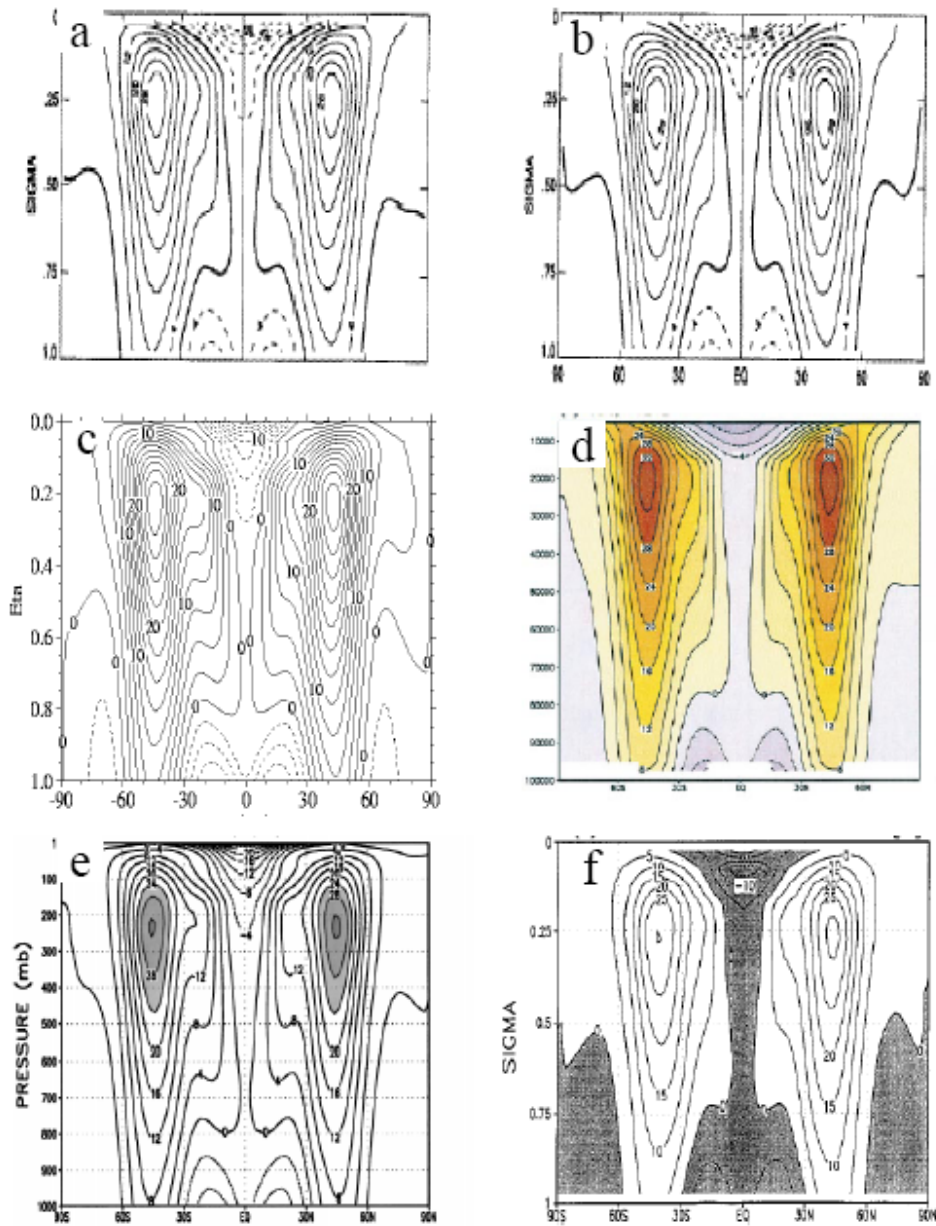
Figure 25   Zonal-mean zonal wind (ms⁻¹) in the Held-Suarez test simulated by some global
atmospheric models:
(a) the spectral model in Held and Suarez (1994) (Contour interval: 4 ms⁻¹)
(b) the grid point model in Held and Suarez (1994) (Contour interval: 4 ms⁻¹)
(c) the GME model in Jablonowski (1998) (Contour interval: 2.5 ms⁻¹)
(d) the geodesic grid model in Ringler et al. (2000) (Contour interval: 4 ms⁻¹)
(e) the finite-volume model in Lin (2004) (Contour interval: 4 ms⁻¹)
(f) the GEOS GCM in Chen et al. (1997) (Contour interval: 5 ms⁻¹).
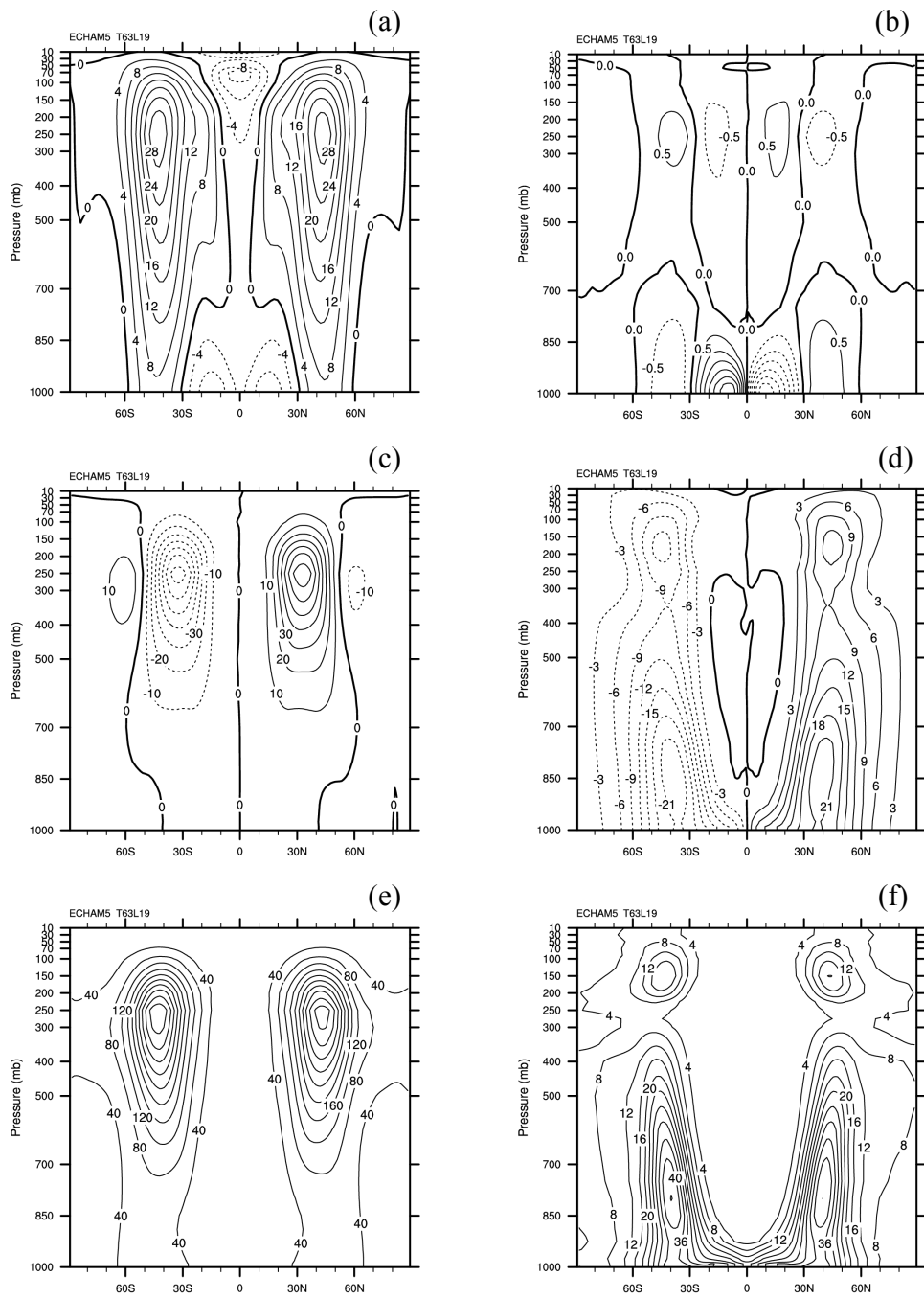
Figure 26   Zonal mean zonal wind (a), meridional wind (b), eddy momentum flux (c) eddy
           heat flux (d), eddy kinetic energy (e) and eddy temperature variance (f)
           simulated by ECHAM5 at T63L19 resolution. The statistics are calculated over
           the last 1000 days of a 1200-day integration.
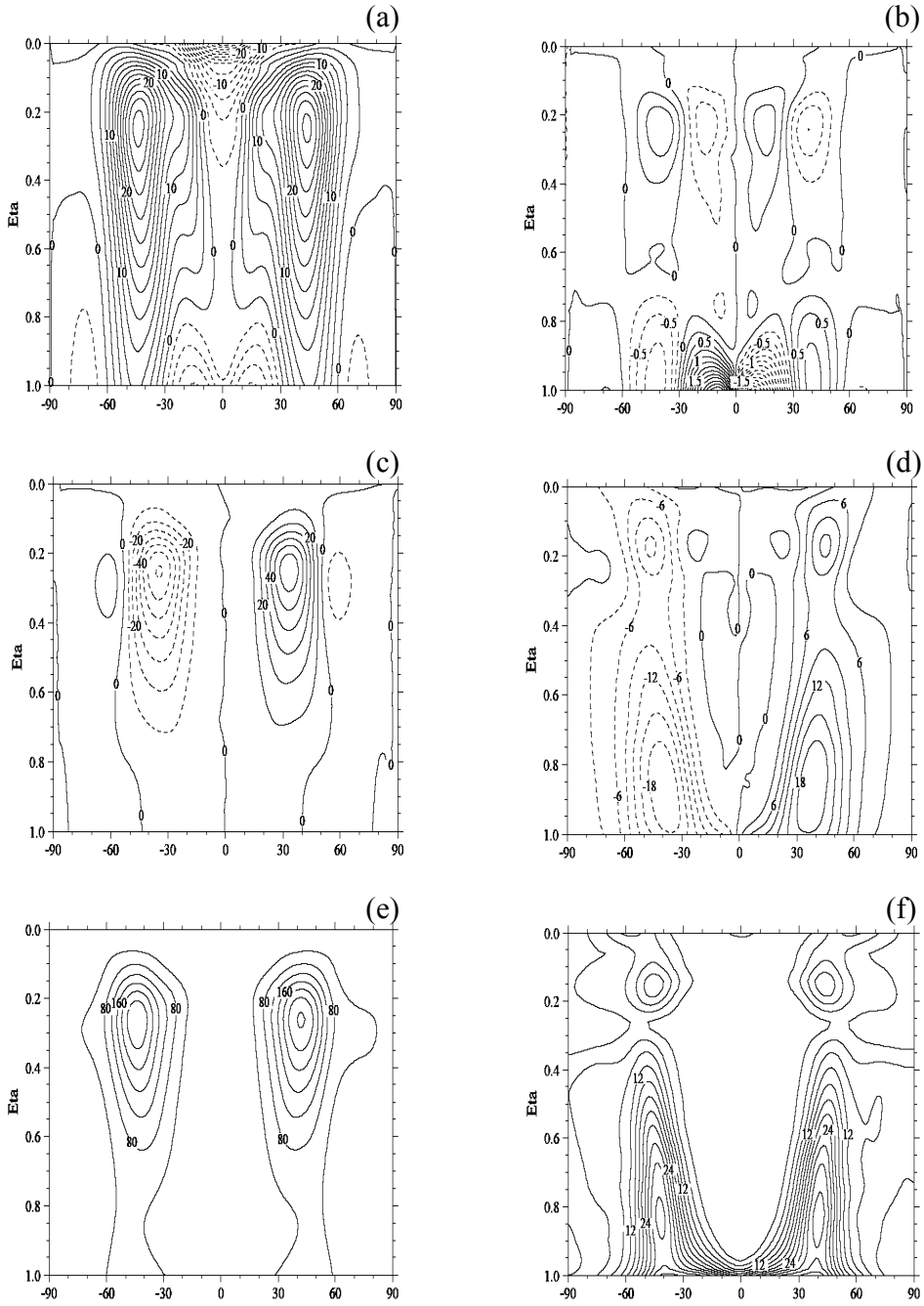
Figure 27   As in Figure 26 but simulated by the GME model at ni=32 resolution. (From Jablonowski 1998). The statistics are averages of ten 90-day periods.
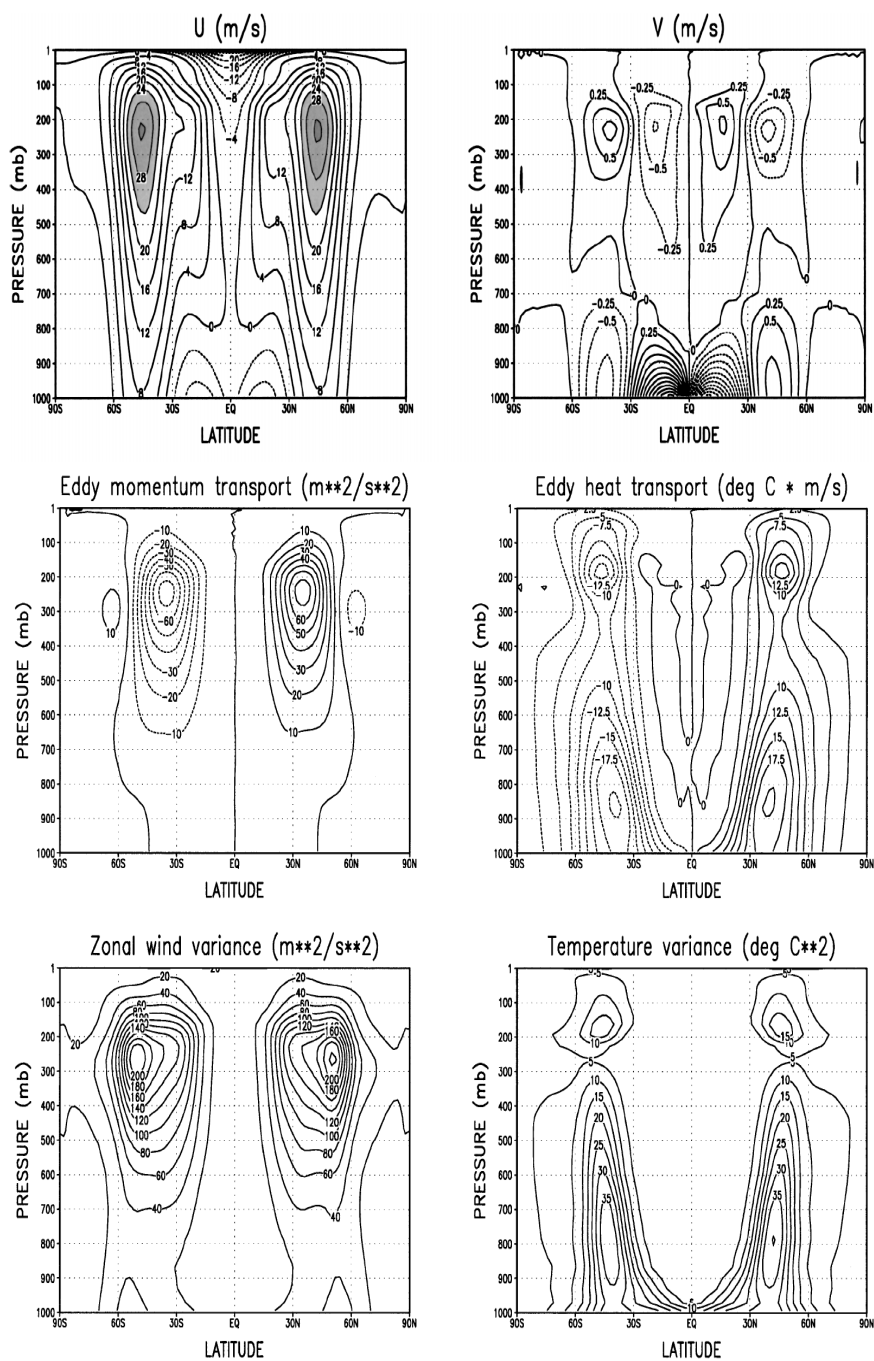
Figure 28   Climate state simulated by the finite-volume model of Lin (2004) at 2°x2.5° resolution with the Held-Suarez forcing. (From Lin 2004). The statistics are calculated over the last 1000 days of a 1200-day integration.

Beginn einer neuen Veröffentlichungsreihe des MPIM, welche die vorherigen Reihen "Reports" und "Examensarbeiten" weiterführt:

**"Berichte zur Erdsystemforschung" , *Reports on Earth System Science*", ISSN 1614-1199
Sie enthält wissenschaftliche und technische Beiträge, inklusive Dissertationen.**

Berichte zur Erdsystemforschung Nr.14
August 2005

The HAM**burg** O**cean** C**arbon** C**ycle Model HAMOCC5.1 - Technical Description Release 1.1**
Ernst Maier-Reimer, Iris Kriest, Joachim Segschneider, Patrick Wetzel

Berichte zur Erdsystemforschung Nr.15
Juli 2005

Long-range Atmospheric Transport and Total Environmental Fate of Persistent Organic Pollutants - A Study using a General Circulation Model
Semeena Valiyaveetil Shamsudheen

Berichte zur Erdsystemforschung Nr.16
Oktober 2005

Aerosol Indirect Effect in the Thermal Spectral Range as Seen from Satellites
Abhay Devasthale

Berichte zur Erdsystemforschung Nr.17
Dezember 2005

Interactions between Climate and Land Cover Changes
Xuefeng Cui

Berichte zur Erdsystemforschung Nr.18
Januar 2006

Rauchpartikel in der Atmosphäre: Modellstudien am Beispiel indonesischer Brände
Bärbel Langmann

Berichte zur Erdsystemforschung Nr.19
Februar 2006

DMS cycle in the ocean-atmosphere system and its response to anthropogenic perturbations
Silvia Kloster